LIPOSOME-COATED METAL ORGANIC FRAMEWORKS

AS A NEW DRUG NANOCARRIER

by

Omnia A. Mohamed

A Thesis presented to the Faculty of the
American University of Sharjah
College of Engineering
In Partial Fulfillment
of the Requirements
for the Degree of

Master of Science in
Biomedical Engineering

Sharjah, United Arab Emirates

December 2019

Approval Signatures

We, the undersigned, approve the Master's Thesis of Omnia A. Mohamed

Thesis Title: Lipsome-coated metal organic frameworks as a new drug nanocarrier.

Signature	Date of Signature (dd/mm/yyyy)
_____	_____

Dr. Rana Sabouni
Assistant Professor, Department of Chemical Engineering
Thesis Advisor

_____   _____

Dr. Ghaleb Husseini
Professor, Department of Chemical Engineering
Thesis Co-Advisor

_____   _____

Dr. Amani Al-Othman
Associate Professor, Department of Chemical Engineering
Thesis Committee Member

_____   _____

Dr. Wael Abuzaid
Assistant Professor, Department of Mechanical Engineering
Thesis Committee Member

_____   _____

Dr. Hasan Al Nashash
Director, Biomedical Engineering Graduate Program

_____   _____

Dr. Lotfi Romdhane
Associate Dean for Graduate Affairs and Research
College of Engineering

_____   _____

Dr. Naif Darwish
Acting Dean, College of Engineering

_____   _____

Dr. Mohamed El-Tarhuni
Vice Provost for Graduate Studies

Acknowledgement

I would like to express my sincere gratitude to my thesis advisor Dr. Rana Sabouni for her continuous support and guidance throughout my research. I would also like to extend my gratitude to My thesis Co- advisor Dr.Ghaleb A. Husseini for his encouragement and motivation. I would also like to thank my thesis committee: Dr. Amani Al-Othman and Dr.Wael Abuzaid for their insightful comments and encouragement.

I would like to thank my family: my parents and my brothers and sister for their emotional support throughout my two years journey at AUS. I would also like to thank my friends, who continuously supported me throughout the past two years namely Mazin, Razan, Nihal, Zahra, Maryam, Fatima, Mawadah, Babiker, Ibrahim and Eman. I want to thank my fellow colleagues at AUS, namely Nour, Afifa, Abdullah and Ibtihal for their help and for the support whenever I felt like giving up.

Very special gratitude goes out to Dr. Hasan Al-Nashash for giving me the opportunity to do my masters at AUS and for his feedback and support.

Finally, I would like to acknowledge the American university of Sharjah for providing me with a graduate teaching assistantship, that allowed me to pursue my Graduate degree.

Dedication

To my family

and friends

Abstract

Cancer has emerged to become one of the predominant diseases ever known to humanity, with chemotherapeutic agents as leading methods for treating it. However, this blind-sighted treatment method that targets all cells; healthy and cancerous, has led to a broad spectrum of side effects that include fatigue, hair loss, nausea and even heart problems. Although potential drug nanocarriers are currently used in the market, e.g., liposomes, yet, their drug loading capacity is still a challenging aspect limiting their usage. This work aims to investigate the development of a novel hybrid nanocarrier from liposomes and Metal-Organic Frameworks (MOFs). In this work, a successful coating of MOFs with liposomes was established by fusion during the preparation of the liposomes. The liposomal coating was verified using several techniques namely, Dynamic Light Scattering (DLS), Cryogenic transmission electron microscopy (Cryo-TEM) and zeta potential. DLS measurements showed a change in the diameter of liposomes from 150±0.82 nm to 163.1±2.16 nm for coated MOFs. Cryo -TEM also showed an increase in the diameter from 155.55 nm for Fe-BTC MOFs and 169.23 nm for coated MOFs. The zeta potential showed charge difference of unloaded, loaded and coated MOFs from a high negative value of -39.33±0.42 mv for loaded MOFs to a relatively neutral charge of 6.23±0.47 mv for coated MOFs. Low-frequency ultrasound (US) at 35 kHz was used as a stimulus to trigger drug release from coated and uncoated MOFs. The ultrasound triggered release reached up to 70% and 50% for coated and uncoated MOFs, respectively. Furthermore, comparing release profiles with and without US, showed statistically significant difference indicating that US can drastically increase the drug release. The effect of US on MOFs structure in terms of crystallinity and composition was analyzed via Fourier Transform Infrared (FTIR) and X-ray powder diffraction (XRD). The FTIR patterns showed a significant change in some of the pore bonds, thus indicating that US alters some pores in the MOFs. The XRD patterns showed that the ultrasound maintained the crystallinity of the MOFs. Further modelling of the release kinetics with ultrasound for both coated and uncoated MOFs was conducted.

Keywords: Drug delivery, cancer, liposomes, metal-organic frameworks, ultrasound

Table of Contents

9

List of Figures

List of Tables

List of Abbreviations

CRYO-TEM	Cryogenic transmission electron microscopy
DLS	Dynamic Light Scattering
DPPC	Dipalmitoylphosphatidylcholine
Fe-BTC	Iron 1,3,5-benzenetricarboxylate
FTIR	Fourier Transform Infrared
MOFs	Metal Organic Frameworks
NP	Nanoparticle
PEG	Poly-ethylene Glycol
PBS	Phosphate Buffer Saline
RES	Reticuloendothelial System
SUV	Small Unilamellar Vesicle
TEM	Transmission electron microscopy
TGA	Thermogravimetric analysis
ULV	Unilamellar Vesicle
US	Ultrasound
XRD	X-ray powder diffraction

Chapter 1. Introduction

Cancer is defined as a group of abnormal cells that goes into intractable growth inside the body. All cells in our bodies have specific functions to do; normally the human cells go into an orderly cellular division. For instance, a cut is healed because the cells in the skin respond to a signal triggering them to divide and form new cells which will fill the injured area. Once the skin is healed the cells respond to another signal that triggers the cells to stop dividing. When cells are worn out, damaged or are dead, new cells take their place. However, cancerous cells keep on dividing, making new cells and crowd out healthy cells where in that part of the body cancer starts [1]. Cancer is a genetic disease, in which mutations occur in the genes that control our cellular function in specific growth and division. These genetic mutations can either be inherited from our parents or evolved during a person's lifespan due to damage in the DNA caused by the external environment; such as exposure to chemicals and ultraviolet radiation from the sun [2].

In a broader concept, most cancers form solid tumors, which are masses of tissue. However, leukemia, which is cancer of the blood, does not generally form solid masses. The difference between a malignant (cancerous) tumor and a benign (noncancerous) tumor; is noncancerous tumors do not travel throughout the body. In contrast, cancerous tumors can spread or seize nearby tissues; some are even able to invade other places in the body to form secondary tumors, which are known as metastases [3].

As most cells undergo cellular division, chaos in cell division can occur, which is the reason for over 200 types of cancer. The name of the organ or the tissues where cancer evolves usually determine the type of cancer, which are far too numerous to include here. The major general types of cancer are carcinoma, sarcoma, leukemia, lymphoma, and myeloma and central nervous system cancers.

Cancer remains one of the deadliest diseases known to humanity and is still on an ongoing battle of treating it since Hippocrates' (father of medicine) time till now (post-genomics era). It escalated to become a significant health hazard at a global level, threatening both developed and undeveloped countries. In 2015 cancer was declared as the second leading cause of death (after cardiovascular diseases) with lung cancer, liver cancer, colorectal cancer, stomach cancer and breast cancer as major primary cancers,

respectively [4]. In 2018, American cancer society estimated there will be 1,735,350 new cancer cases and 609,640 cancer deaths in the U.S. by 2018, which translates to about 1,670 deaths per day. The appalling rates of cancer were not different in the Middle Eastern region, with world health organization (WHO) estimating it to be highest relatively in a number of cancer cases of all regions in the world by 2030 [5].On a more specific level, in United Arab Emirates cancer is the third leading cause of death in the emirate of Abu Dhabi. Figure 1 indicates the frequent cancers in Abu Dhabi, UAE 2014 [6].
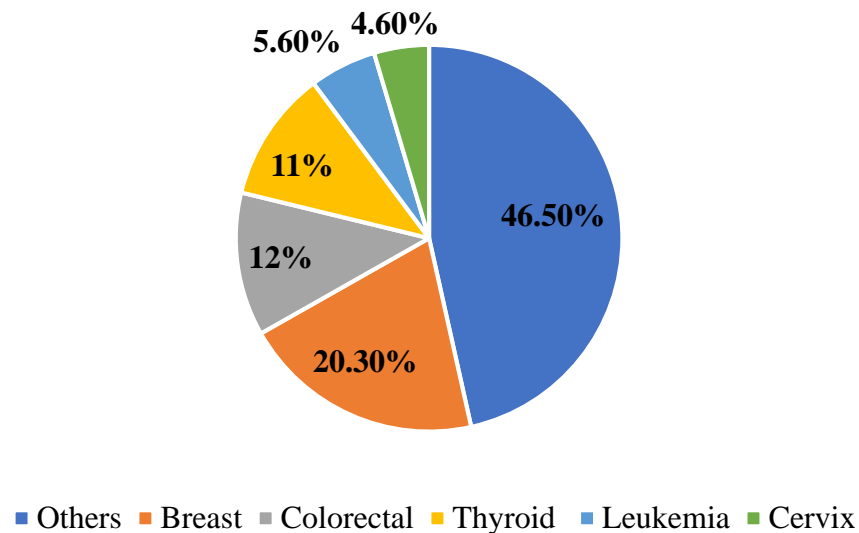
Figure 1: Common cancers in Abu Dhabi 2014 [6].

Many techniques have emerged to cure cancer, with a basic concept to cease the cellular division of these cancerous cells. The most common cancer treatments used today include surgery, radiotherapy, and chemotherapy. Many factors determine the appropriate therapy method for cancer, and a combination of techniques is often used. Surgery and radiotherapy have monopolized cancer treatment field for a long time. However, surgical methods only eliminate clear bounded tumors and radiotherapy is often a follow-up therapy used to banish cancer cells missed by the surgeon's scalpel. Chemotherapy emerged, as some cancer tumors are challenging to resect or they become immune to radiotherapy [7].

Chemotherapy exploits cytotoxic agents that interrupt the cellular division process and cause cancer cells death by either damaging the DNA or proteins in the cells that are essential for cellular division. This form of therapy targets both normal and cancer cells, basically any rapidly dividing cells. Though normal cells can heal

from any chemical damages, cancer cells do not; they therefore die. There are diverse cytotoxic agents used in chemotherapy which include alkylating agents, antimetabolites, anti-tumor antibiotics, topoisomerase inhibitors and tubulin-binding drugs. These drugs, once induced into the body, should circulate through the body, avoiding defense mechanisms and encountering the tumor. Nevertheless, the majority of these drugs do not complete this cycle and end up either ineffective or toxic to the patient. Infective chemotherapy occurs when some cells mutate and become resistant to the drug. Furthermore; rapid cellular division induces more cells that are resistant to chemotherapy. The toxicity of chemotherapy lies in the fact that it is an unanchored treatment method. As a result, healthy and cancer cells are both interrupted causing severe side effects, such as nausea, vomiting, hair loss, acute cholinergic gastrointestinal effects and heart problems (cardiac toxicity) [7], [8].

These blind-sighted techniques, which cannot discriminate healthy and unhealthy cells nor localize the drugs in the diseased regions of the body has led to the development of novel drug carriers. This thesis investigates the development of hybrid novel drug carriers, namely liposomes coated Metal organic frameworks (MOFs) as a potential drug delivery system carrier that can surpass the limitations of many current novel carriers.

Chapter 2. Literature Review

2.1. Drug Delivery Systems

Drug delivery is defined as the methods, approaches and technologies involved in administrating therapeutic compounds into biological systems such as humans [8]. Drug delivery systems can be further divided into conventional drug delivery and novel drug delivery. Conventional drug delivery systems are the classical methods of delivering drug into the body which includes:

Oral: The drug is delivered through the mouth. It is the most preferred method because it is highly acceptable by the patient, however, it has some drawbacks such as the uncertainty of the absorption. Also, the drug has to resist the digestive system enzymes and penetrate to the bloodstream [9].

Transdermal: The drug is delivered through the skin. Despite its convenient, pain-free and self-administration for patients, it restricts drug option and requires significant time [10].

Transmucosal: The drugs can be administrated either via a nasal route or oral (under the tongue)/buccal route. It offers the advantages of evading some of the body's defence mechanism, yet it is limited to small doses drugs [11].

Pulmonary: The drug is inhaled into the lungs. The high surface area of the lungs offers an extensive site for absorption, but the efficacy of the drug depends on the specific ejection site within the lung [12].

Intravenous injection: The drug is injected into the veins. Although it is the most efficient means of delivering the drug, yet the complications and adverse events associated with it restrict its application [13].

Due to the numerous drawbacks of the conventional drug delivery systems, a need has emerged for novel smart drug delivery systems that achieve the full therapeutic drug potential. The section below presents some of the novel drug delivery systems that include but not limited to liposomes, metal organic frameworks and hybrid liposome-metal organic frameworks.

2.2. Novel Drug Delivery Systems

Novel drug delivery systems integrated polymer science, pharmaceutical technology, bioconjugate chemistry, and molecular biology capitalizing on ideas of controlling the pharmacokinetics, pharmacodynamics, immunogenicity, and

biorecognition to achieve drug efficacy [14]. Various Nano-systems are utilized to deliver the drug to the intended sites including nanoparticles, nanosponges, liposomes, dendrimers, micelles and cyclodextrins [15]. Those nano-systems offer optimized drug loading, enhanced drug efficacy and bioavailability, lower toxicity and can be further modified to target the required zone [16]. Drug targeting is the ability of the drug to accumulate in the target area which can be either a tissue or an organ, providing a continuous supply of therapeutic drugs [17]. There are three major mechanisms of drug targeting which are passive, active and triggered mechanism.

      2.2.1. Passive targeting. Drug efficacy depends on circulation time and the leaky vasculature areas around tumors that offer accumulation at targeted sites on the count of enhanced permeability and retention (EPR) phenomenon, Figure 2. Circulation time can be increased by evading the immune system, which can be achieved by controlling certain parameters of the nanocarriers notably size and surface. Usually, nanocarriers having less than 200 nm size have significantly longer circulation times. More recently it was reported that the optimum diameter for a spherical nanocarrier to avoid clearance is 150 nm [18]. Surface modification is attained by the incorporation of several substances such as polyethylene glycol (PEG). Such substances alter the surface of nanoparticles to evade opsonization by the reti-culoendothelial system [19], [20].

      2.2.2. Active targeting. It is similar to passive targeting in the sense that nanocarriers also localize in cancer cells. However, it is further modified to interact specifically to the tumor cells by attaching a ligand that targets specific receptor at the tumor cells ,Figure 3. The overexpression of tumor cells to specific receptors determine the type of ligand that will be attached to the nanoparticle such as antibodies and their variable fragments, peptides, folate, vitamins, and carbohydrates [21],[22].
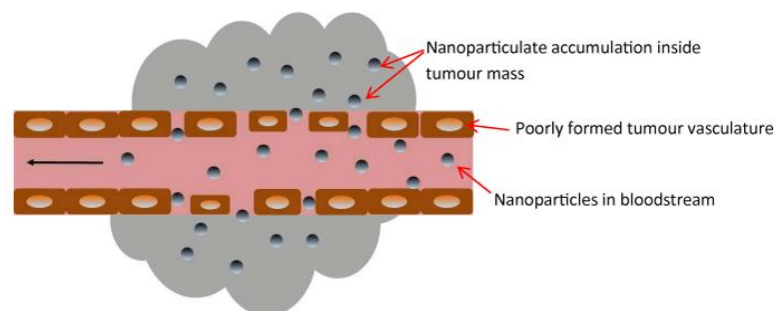
Figure 2: EPR effect in blood vessels near cancer cells [23].
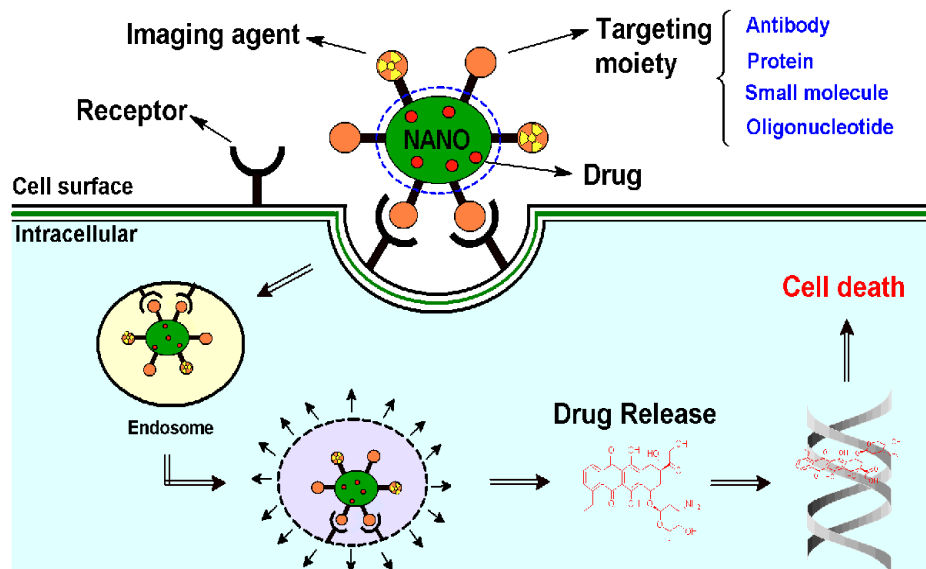
Figure 3: Active targeting schematic [24].

2.2.3. Triggered mechanism.

2.2.3. Triggered mechanism. The difference in the environment surrounding cancer sites compared to normal cells, has attributed to several factors that can be utilized as to release the drug from nanocarriers. They can be internal such as pH, redox, enzyme, temperature, etc or external such as temperature, light, ultrasound, magnetic fields, etc. [25]. Enzymes are selective to certain linkers. For example, peptides can trigger proteases and polysaccharide can trigger glycosidases. This serves as the base for triggered release. Meaning the degradation of the nanocarrier is prearranged according to the enzyme sensitivity [26]. External triggering is even more selective as it controls both the nanocarrier mobility and release. Magnetic fields have been reported to direct and localize iron oxide nanoparticles to cancer sites [27]. This indicates the possibility of combining several triggering factors to incorporate the drug release and localization.

2.3. Liposomes

Liposomes are spherical vesicles composed of one or more phospholipids bilayers; they serve as drug delivery vehicles [28]. Liposomes are amphiphilic molecules having a hydrophilic head which is mainly phosphoric acid bound to a water-soluble molecule and two hydrophobic tails consisting of fatty acid chains. They align themselves in a thin sheet-like structure with heads facing aqueous region while the tails face each other, thus forming the bilayer spherical form when dispersed in an aqueous medium as shown in Figure 4 [29]. Liposomes have become one of the major

pharmaceuticals carriers that have a high potential owing to their biological advantages including biodegradability, biocompatibility and tunability in terms of size, and ability to entrap soluble and insoluble drugs and modify charge and surface properties by altering the lipid composition [30].
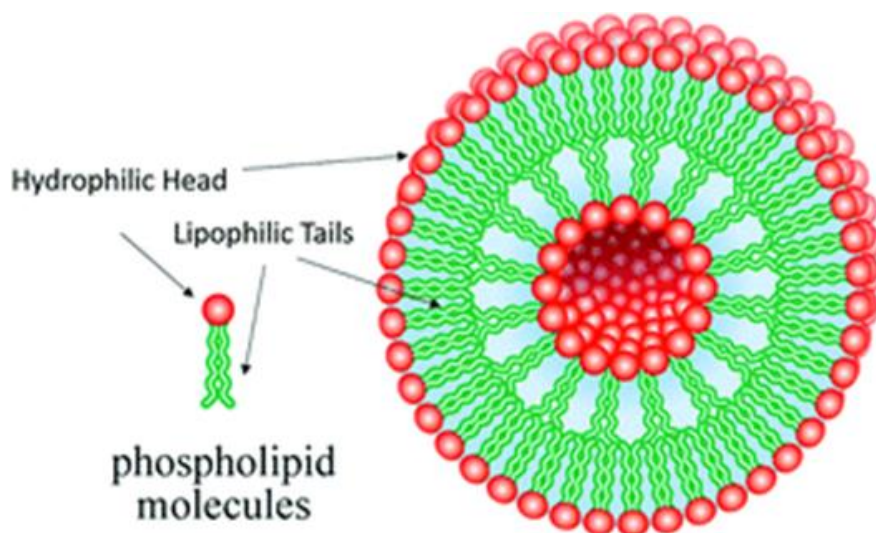
Figure 4: Schematic of a liposome structure [31].

2.3.1. Classification of liposomes. Liposomes can be classified according to the size or the composition.

- On the size basis

Liposomes size vary ranging from very small (25 nm) to large (2.5 μm). It is an essential factor to be considered as a criterion of the circulation time as mentioned earlier. Liposomes can also have one or a number of bilayers which discrete them in two categories: (1) multilamellar vesicles (MLV) having more than one lipid bilayer and (2) unilamellar vesicles having one lipid bilayer which are further classified into two categories 1) large unilamellar vesicles (LUV, >100nm) and (2) small unilamellar vesicles (SUV,<100 nm) [29], [30].

- On the composition basis

Liposomes are composed of natural or synthetic lipids that have a pronounced effect in determining the interaction of liposomes and cells. The net physicochemical properties of the lipids comprising liposomes determine the membrane fluidity, charge density, steric hindrance, and permeability [32]. Table 1 lists typical composition-based liposomes and their characteristics.

Table 1: Liposomes classification based on composition and their characteristics [27].

Type	Characteristics
Conventional liposomes	Neutral or negatively charged phospholipids plus cholesterol.
pH-sensitive liposomes	Stable at physiological pH but are destabilized upon acidification following cellular internalization, thereby, promoting the release of their contents into the cytosol
Cationic liposomes	Their cationic lipid components interact with, and neutralize, the negatively-charged DNA, thereby they are being researched in gene therapy.
Immuno -liposomes	Have specific antibodies or antibody fragments on their surface to enhance Target site binding.
long-circulating liposomes	Coating of the surface by hydrophilic compounds, currently the most common is conjugating the hydrophilic polymer polyethylene glycol (PEG) covalently to the outer surface of the liposomes.

2.3.2. Parameters influencing the behavior of liposomes. The ability of liposomes to effectively deliver the encapsulated drugs to the target cells and effectively perform its therapeutic requirements can be optimized in term of drug content, stability, desirable biodistribution patterns, and cellular uptake. Altering the physicochemical parameters includes the fluidity of bilayer membrane, surface charge density, surface hydration and size [32].

- Bilayer fluidity

The lipid bilayer of the liposomes has a unique property which is fluidity (relative mobility), and this fluidity changes with a phase transition temperature. Lipids below this temperature exist as well-ordered arranged solids, and above this temperature, they exist as liquid crystalline fluid. Thus, the fluidity of liposomes is controlled by the transition temperature of the lipids it is composed of. This plays a critical role in the immune system response of liposomes and circulation time as it is noted that liposomes with high transition temperature have a lower uptake by the immune system compared to those with lower transition temperature [33]. Furthermore,

including cholesterol in the lipid bilayer formulation seems to add more rigidity to the liposomes and prevent premature release [34].

- Surface charge density

The surface charge of liposomes plays a crucial role in their cellular uptake and how the drug enters the cell [35]. Negatively charged liposomes have a higher uptake by endocytosis compared to neutral liposomes. In vivo studies have shown that such liposomes stimulate uptake through interaction with serum proteins [36], however, as they can interact with serum proteins, forming opsonins that can drastically be eliminated from the body [37]. While neutral liposomes lack the specific interaction with cells and the drug usually enters after extracellular release from liposomes [38]. On the other hand, positively charged liposomes deliver drugs by fusion with the cell membrane, but the cytotoxicity has been the main hindrance in their usage as drug carriers. They induce an inflammatory response in the cells because they interfere with the potassium-sodium solute pump of the cells membranes which leads to cell death [39].

- Surface hydration

The efficacy of a liposomal drug delivery system depends mainly on long circulation time; this is directly related to bypassing the immune system. The surface engineering of liposomes has been a breakout in the development of stealth liposomes. It offers liposomes the invisibility attribute by coating the outer surface of liposomes by stealth improving properties substances. As a result, these modified liposomes are prevented from binding and recognition by plasma proteins [40]. The incorporation of substances with hydrophilic groups such as monosialoganglioside (GM), hydrogenated phosphatidylinositol (HPI) and polyethylene glycol (PEG) forms a layer close to the liposomes which hinders their uptake by blood plasma [41].

2.3.3. Methods of liposomes preparation. All the preparation methods of liposomes include fundamental steps: Drying down the lipids in an organic solvent, dispersing the lipids in an aqueous solution, purifying the resulting liposomes and analyzing/characterizing the final product [30]. The difference in the fundamental steps leads to the various preparation techniques of liposomes

2.3.3.1. *Thin film hydration method.* This is one of the simplest methods to prepare liposomes; a mixture of lipids is dissolved in an organic solvent which is later

removed by means of evaporation to make a thin lipid film. Hydration is followed up at constant stirring at a temperature higher than the lipids transition temperature [42].

2.3.3.2. *Reverse-phase evaporation.* This method was first described by Szoka and Papahadjopoulos; it is based on composing inverted micelles. This method depends on the slow elimination of inverted micelles that are in an aqueous solution containing encapsulated molecules and an organic solvent. The use of sonication leads to transforming these inverted micelles into a gel form which further disintegrates remaining phospholipids that surround the remaining micelles and form the remaining bilayer, thus making the bilayer liposomes [30].

2.3.3.3. *Solvent injection technique.* This method involves the dissolving of the lipids by an organic solvent which is injected into an aqueous solution containing the encapsulated molecules. The organic solvent is continuously removed under evaporation and reduced pressure. These methods offer simplicity and small size liposomes but with a heterogeneous nature and a full size distribution [30].

2.3.3.4. *Detergent dialysis (removal of non-encapsulated material).* The lipids are solubilized by a detergent, forming micelles. As the detergent is removed by dialysis, micelles lose their bounded detergent molecules, and phospholipids align to form liposomes [43].

2.3.4. Limitations of liposomes. The liposome drug delivery system manages to overcome many of the traditional chemotherapy barriers. It offers the sustained predetermined release rate, localizes drug action in the desired tissue and addresses the concerns of toxic drugs, however, it is still inadequate in some aspects [44]. From the physical point of view, liposomes are still unstable and can aggregate and fuse together without retaining their size distribution, which can impact their shelf-life as the drug might leak and undergo reactions within the liquid in which liposomes are stored. At a chemical level, phospholipids might undergo oxidation of unsaturated fatty acid chains and the hydrolysis of the covalent bonds that conjugate the fatty acid to the glycerol, thus, affecting the fatty acid chain length which eventually influences the liposomes quality. Sterilization of liposomes is still an issue as most sterilization processes either require high temperatures which can result in degradation of liposomes, lack of conveniences such as gamma radiation and saturated steam or have high cost such as filtration and denes gas techniques [45]. The large-scale production of liposomes, as clinically approved drug carriers, is still governed by the high costs associated with the

raw materials and manufacturing process. The typical method of forming large vesicles, then downsizing by sonication, cannot serve in large-scale production and is limited only to laboratory small-scale production [46].

2.3.5. Therapeutic application of liposomes in drug delivery. The first application of liposomes as drug carriers was Doxil in 1995. Doxil is the drug doxorubicin encapsulated in a liposome. It has several advantages: Over free doxorubicin includes prolonging circulation time, invisibility to the immune system, high and stable loading and having liposomes bilayer at high transition temperature (53 °C). However, Doxil mainly employs the passive targeting method which relies on the enhanced permeability and retention (EPR) effect [47]. Table 2 summarizes some of the current approved and used liposomes-based drug carriers.

Table 2: Liposome-based drugs on market [43].

Product name	Route of injection	Drug	Particle type	Drug form/Storage time	Approved indication
DaunoXome	Intravenous	Daunor	Liposome	Emulsion/12 months	Blood tumors
Doxil	Intravenous	DOX	PEGylated liposome	Suspension/20 months	Kaposi's sarcoma, Ovarian/breast cancer
Lipo-dox	Intravenous	DOX	PEGylated liposome	Suspension/36 months	Kaposi's sarcoma, ovarian/breast cancer

2.4. Metal Organic Frameworks (MOFs)

Metal organic frameworks are hybrid crystalline materials, which are composed of organic units (negatively charged linkers) such as ditopic or polytopic organic carboxylates and inorganic units (metal cations). This crystalline construction offers an open porous structure that gives a high porosity and high surface area to MOFs in comparison to others such as zeolites and carbons. Typical pore sizes range up to 2

nm which accommodates small molecules. Though, a variation of the metal ions or organic ligands can induce a larger pore size [48]. The investigation of MOFs as potential drug carriers emerged from the fact that they have a flexible structure in a sense that during the synthesis process alteration during it can affect the pore size and shape to accommodate the molecule to be encapsulated in the pores [49]. MOFs also attain the other properties that are required for a successful drug delivery system. They encounter high loading capacity, high chemical, thermal stability, controlled drug release properties, biocompatible, and ease of surface modification with attaching functionality groups [50].

2.4.1. Brief history of MOFs. The field of MOFs emerged from the study of zeolites which are crystalline solids structures entirely made of inorganic materials. It initiated the interest in achieving porous coordinated structures. Around 1995, a pioneering material chemist Omar Yaghi introduced the term MOFs. He and his coworker were able to synthesis MOF-5 as shown in Figure 5, which consists of ZnO_4 units connected by the 1,4-benzenedicarboxylateligand to form a cubic crystalline network [51]. Since then the development and study of MOFs have expanded the high porous structure, low density and the ability to tailor them during the synthesis process which has led to their versatile applications including gas storage and separation, drug delivery, luminescence, or heterogeneous catalysis. The diversity of the linkers and metals that can form MOFs has led to multiple names associated with MOFs on the basis where they are first discovered as in HKUST (Hong Kong University of Science and Technology) or and MIL (Materials Institute Lavoisier).
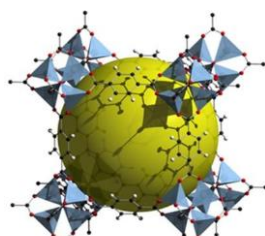
Figure 5 : MOF-5 where ZnO_4 tetrahedra (blue polyhedra) joined by benzene dicarboxylate linkers (O, red and C, black) to give an extended 3D cubic framework with yellow sphere representing the pore area [48].

2.4.2. Classes of MOFs. MOFs are a class of solid porous materials. They represent the thin line between organic porous materials (e.g. polymers) and inorganic

porous materials (e.g. zeolites). They can be classified according to how the unit cells align themselves as shown in Figure 6.

- Crystalline MOFs

The building units align in an ordered manner, thus having a repeated pattern and a defined shape [52].

- Amorphous MOFs:

The building units align themselves in a disordered manner. They tend to lack an exact shape, and they are crystals that have collapsed due to temperature, pressure and ball milling [53].
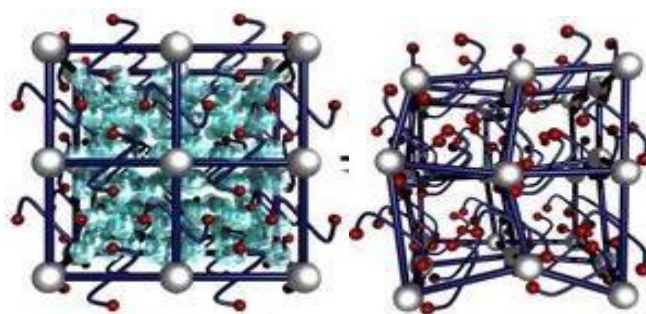
Figure 6: Crystalline MOF to the left and an amorphous MOF to the right.

According to International Union of Pure and Applied Chemistry (IUPAC), MOFs can also be classified according to the pore size as either microporous (pore sizes <2 nm) and Mesoporous (pore size: 2–50 nm). Up until now, most of the reported MOFs fall under the microscale pore size with a smaller fraction of MOFs in mesoporous category [54].

2.4.3. Synthesis of MOFs. The most common synthesis route for MOFs is solvothermal or hydrothermal in which metal salts and ligand solutions are mixed, and a solvent is added, followed by rounds of electrical heating to promote the self-assembly. Reaction time varies from several hours to days. However, this was overlooked as the main effort targeted at the achievement of high-quality crystalline structures. Other routes of synthesis are being considered such as solid-state synthesis, yet it still produces MOFs with an amorphous structure [55]. Some of the most common solvothermal synthesis methods will be discussed in this section.

2.4.3.1. *Slow evaporation method.* It is the conventional method to prepare MOFs: metal salts and organic ligands are mixed with a solvent and time is allowed for the reaction to proceed. Afterwards, the solvent is removed gradually by the simple drying of the solvent exchange. This method is one of the simplest because it does not require any electrical heating, yet it is one of the slowest methods [55]. Some of the most well-known MOFs are synthesized by this method such as MOF-5, MOF-74, MOF-177, HKUST-1 or ZIF-8 [51].

2.4.3.2. *Solvothermal synthesis.* The metal salts and organic ligands along with the solvent at a temperature higher than its boiling temperature are reacted in closed vessels under high pressures. Solvothermal synthesis promotes the nanoscale MOFs as it plays an important role in stabilizing the denser structures (MOFs) and enhancing the chemical reactivity and the kinetics of the involved reactions [56].

2.4.3.3. *Microwave-assisted synthesis.* It is the rapid method for MOFs synthesis; it offers a more uniform MOFs with a small polydispersity index, and has been used in the commercial production of MOFs [57]. It involves the heating of reactants along with the solvent. The electromagnetic radiation triggers the dipole molecules usually at the ligands resulting in a faster reaction and higher product yield [58]. Cr- MIL-100 was the first microwave synthesized MOF, 44% yield was achieved in four hours compared to a conventional method that required four days [57].

2.4.3.4. *Electrochemical synthesis*. In this method, a galvanic cell with a continuous supply of metal ions coming from an anode metal reacts with organic linkers in the electrolyte solution mixture; this method offers the advantage of continuous production of MOFs[57]. BASF, one of the largest worldwide chemicals producers first reported this method for HKUST-1MOF. Since then this route has been used of synthesis of Zn-based MOFs, Cu-based MOFs, and Al-based MOFs [59].

2.4.3.5. *Sonochemical synthesis.* The ultrasound radiation induces a cavitation phenomenon in which the rapid formation and collapse of bubbles generate a wide temperature changes from high to low. That further induces the formation of MOFs. The main advantage of sonochemical synthesis is that it produces high- quality nanoscale MOFs in a fast manner compared to solvothermal synthesis [57].

3.4.4. MOFs as anti-cancer drug carriers. The outstanding properties of MOFs include: high porosity, large specific surface area, diverse surface functionality, pore size tunability, structural stability, non-toxicity, and biocompatibility, which have

led to investigating them as potential drug carriers. Currently, MOFs as anti-cancer drug carriers are not used in the market mainly due to their low intercellular uptake. However, some of the most promising researches in anti-cancer MOFs will be reviewed.

Lenget et al. investigated the loading and release efficiencies of MIL-53(Fe) for the anticancer drug oridonin (Ori). The MOFs achieved a loading efficiency of 56.25 wt% and a high release up to 82.23% in a 7-day period. Further studies of the cytotoxic effects of Ori loaded MOFs on HepG2 cells compared to free Ori at the same concentrations, showed that Ori loaded MOFs achieved at the same cell viability of the free Ori induce. In contrast, Ori loaded MOFs required a more extended period to induce cell death, thus indicating the slow release of the MOFs and the small cellular uptake [60].

In another study, Jintonget et al. synthesized a multifunctional Metal Organic Framework nanoprobe for Cathepsin B-Activated Cancer Cell I. NH2-MIL-101(Fe) were loaded with the anti cancer drug camptothecine (Cam), followed by surface modification with folic acid (FA) as the targeted element. Further, modified with chlorine e6 (Ce6)-labeled CaB substrate peptide (Ce6- peptide) as the signal and recognition moiety, Figure7.
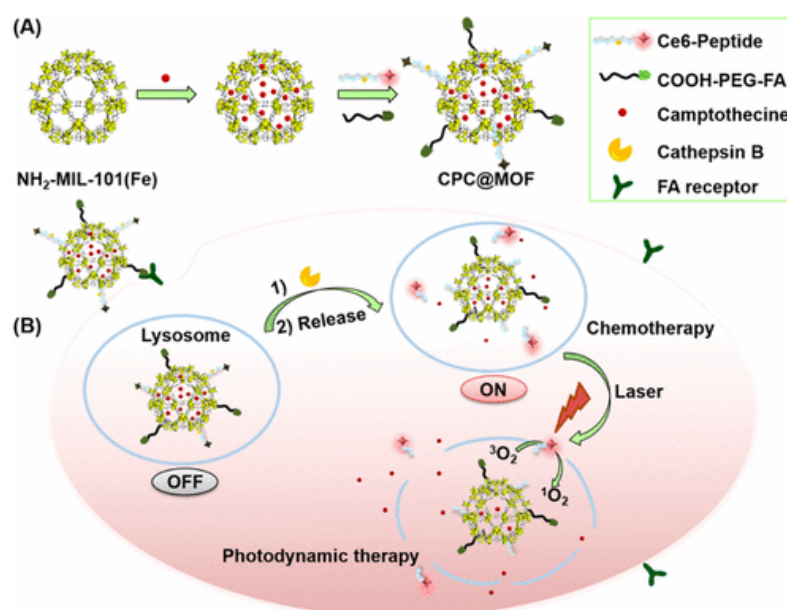
Figure 7: Schematic Illustration of (A) Preparation of Multifunctionalized CPC@MOF Nanoprobe and (B) Cathepsin B-Activated Cancer Cell Imaging and Chemo-Photodynamic Therapy [85].

The successful attachment was confirmed with measuring the cell viability of HeLa cells upon incubation with Ce6@MOF, CPC@MOF. Laser irradiation was utilized to trigger release and measure the success of Ce6-peptide as a photo-sensitizing agent. The CPC@MOF causes cell death of up to 99.27% (Hela cells under laser triggering compared to achieving only 35.17% apoptosis without laser triggering). The laser beam had an insignificant effect on the release of drugs from ce6@MOF without the folate moiety. *In vivo* experiments concluded the success of CPC@MOF as drug delivery vehicles with a heavy accumulation at cancer sites within a maximum at 24 h, Figure 8, and a dramatic decrease in tumor size within a 14-day period compared to other non-targeted carriers, i.e. nanocarriers without the conjugated moieties [61].

Zhengfei et al. loaded the anti-cancer drug doxorubicin hydrochloride (DOX) into meso-iron MOFs and studied their effect *in vivo* and *in vitro*. A loading content of 55 % wt. was achieved, and the loaded meso-MOFs exhibited a stronger anti-tumor effect compared to free doxorubicin in 4T1 breast cancer-bearing mice [62].
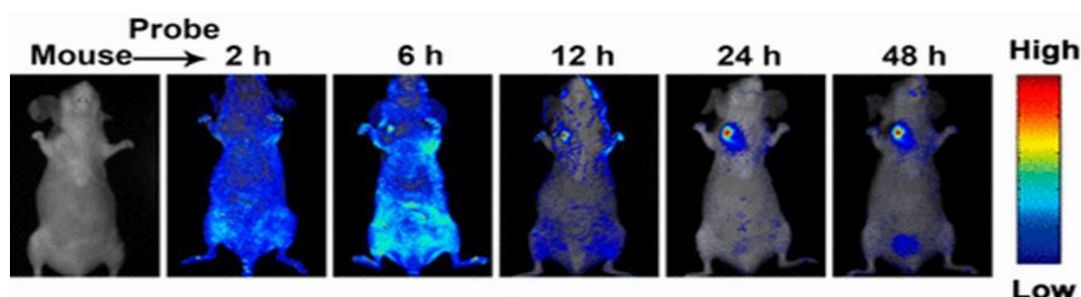
Figure 8: Time-dependent in vivo fluorescence images of subcutaneous HeLa tumor-bearing mouse after injected with CPC@MOF [58].

3.4.5. Hybrid system of MOFs and liposomes. Recent in vitro research managed to prove MOFs as potential drug carriers, surpassing some of the alternatives currently used in term of drug loading capacity. Despite this in vitro success, in vivo studies have not been conducted as extensively. The fast cargo release rate from MOFs, colloidal instability issues and short circulation cycles have limited further researches. The challenges for MOFs as anti-cancer drug carriers have been addressed by the surface modification of MOFs, either by adding functional groups that can improve the stealth of MOFs or encapsulating them by another carrier that have superior stealth properties. Utilizing the liposomes, i.e. the specific encapsulation of the MOFs inside the liposomes, have proven to help achieve the full, true potentials of both carriers.

Previous studies

Bernhard et al. investigated MIL-88A's ability to carry a cocktail of drugs and attempted to control the release by coating the MOFs with a lipid bilayer to act as a seal. The loading capacity of MIL-88A with two chemotherapeutic drugs, namely irinotecan and floxuridine, was studied individually and as a dual drug mixture. The MOFs individual loading capacity for each drug was quantified by soaking 1 mg of MIL-88A in 1 mM solution of irinotecan and comparing the supernatant to a pure 1mM solution of irinotecan using UV/Vis measurements. MIL-88A yielded 21 wt % (relative to the weight of MOFs) for irinotecan. The same procedure was followed for floxuridine yielding 14.7 %. For the mixture of the drugs, a 0.5 mM solution was prepared for each drug and mixed (ratio 1:1) using UV/Vis measurements yielding a loading of 10.3 wt % for irinotecan and 6.9 wt% for floxuridine. These results confirm the effectiveness of MIL-88A as a promising nanocarrier for a cocktail of drugs. To prepare liposomes, a DOPC (1,2-dioleoyl- sn-glycero-3-phosphocholine) lipid solution was prepared. The low transition temperature of DOPC lipids was the reason for usage because at room temperature the lipid bilayer will act as a liquid crystal. Thus, the bilayer is not rigid and can encapsulate the MOFs.To establish the liposomes coating, fluorescence release experiments were conducted on the liposomes coated MOFs. The MIL-88A was loaded with calcein and incubated for 2 hours in the liposomal solution. A sample of the Lip-MIL-88A was used as a test for leakage against uncoated loaded MIL-88A and other samples treated with Triton X-100 and artificial lysosomal fluid (ALF) that induce the rupture of the liposomes coating. The coated MOFs showed no release even after several hours compared to uncoated MOFs that showed a fluorescence increase thus, proving the effectiveness of the liposomes seal as shown in Figure 9. Both the Triton X-100 and ALF treated MOFs showed dramatic release compared to coat untreated MOFs and uncoated MOFs, which is explained by the release of calcein that diffused into the area between the MOFs and the liposomes inner surface. Cell release experiments were conducted to study the uptake of cells to Lip-MIL-88A. Lip-MIL-88A was loaded with calcein and incubated with HeLa cells. It was found that the lysosomes have started breaking up the coated MOF after 2 days and a release of calcein was observed. This established the ability of the hybrid liposomes and MOFs system to conduct a high drug delivery without premature release. Further single and multidrug MTT assays were conducted for Lip-MIL-88A loaded with

irinotecan and floxuridine individually and a mixture of the two drugs using the previously mentioned methods. Multi-drug loaded Lip-MIL-88A reduced cell viability up to 30.6%, surpassing single drug-loaded carriers [63].

Stefanetet et al. studied coating MIL-100 and MIL-101 MOFs by a lipid bilayer using a controlled solvent deposition exchange procedure. DOPC lipids were dissolved in an ethanol and water solution upon increasing the water concentration of the lipids precipitated on the MOFs forming a lipid bilayer. The confirmation of the lipid bilayer was established by Dynamic Light Scattering (DLS) measurements, which showed an increase in the diameter to around 20 nm on average for both MOFs. In addition, time-series DLS measurements showed that the colloidal stability established after 72 hours, since no change in the size distribution was observed. Moreover, the fluorescence release experiments were conducted on both coated MIL-100 and MIL-101 loaded with calcein, no significant release over a one-hour period was observed. In contrast, the addition of Triton X-100 showed a rapid fluorescence increase which confirmed that bilayer localization on the MOFs surface. The localization of the lipid bilayer was further explored utilizing fluorescence confocal microscope. MIL-101 and the lipids were stained with two different fluorescent dyes and a cross-correlation analysis of the fluorescence intensity was conducted, and it showed a high cross-correlation ratio . Furthermore, *in vitro* experiments were conducted to find the cellular uptake of coated MIL-101 by bladder carcinoma. The cellular uptake was detected within 6 hours and lasted for 48 hours [64].
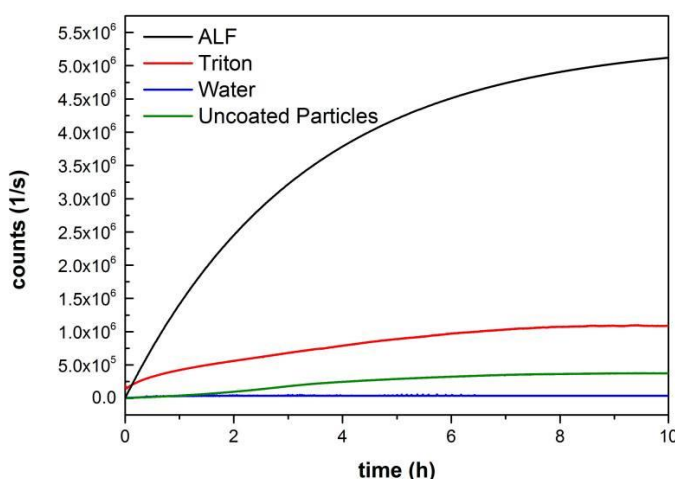
Figure 9: Fluorescence release measurement of Lip-MIL-88A in various solvents. Water (blue) and water with the addition of Triton X-100 (red), as an additional of ALF (black) and uncoated particles (green) [60].

Jian et al. focused on resolving the biological instability of Zr MOFs. The existence of phosphate in most biological system limited the use of Zr MOFs as drug carriers due to the high affinity of phosphate-to-metals compared to the organic linker. Consequently, this affinity can induce a substitution of the organic linkers by phosphate and result in a collapse of the MOFs. Zr-based porphyrinic MOF of PCN-223 was coated by DOPC lipids in two stages; the first stage was dissolving the lipids in chloroform then stirring the resultant solution in the presence of the MOFs for 24 hours which resulted in a monolayer by the attachment of the free oxygen sites on the surface of MOFs to the phosphate group of DOPC lipids. In the second stage, DOPC and cholesterol were dissolved in ethanol, and a water solution, followed by the addition of the monolayer coated MOFs and gradual evaporating of the solvents. The presence of the bilayer on Zr MOFs was confirmed by several methods. FTIR spectrum showed new vibrations corresponding to the P-O bonds and the abundant CH2 groups in the fatty acid chains. Zeta potential measurements indicated that new coated Zr MOFs acquired the neutral electrical charge of the DOPC lipids (-2.7 ± 0.2 mV) compared to uncoated Zr MOFs which had high negative charges (-34.2 ± 1.3) mV. TEM imaging with negative staining using uranyl acetate confirmed the lipid bilayer coating. The uranium and the phosphonate head groups interaction was confirmed using the TEM images of the coated Zr MOFs and a large accumulation of the stain compared to uncoated Zr MOFs.DLS measurements over a seven-day period showed the long-term maintained dispersity index of coated MOFs compared to uncoated MOFs that tended to aggregate within a day. The phosphate resistance property was studied as a measure of the successful coating using TEM, XRD, and UV−vis spectra. Samples from incubation with PBS buffer at pH 7.4 of coated and uncoated MOFs showed a fast degradation of uncoated MOFs compared to coated ones. TEM images showed the degradation of the MOF within two days. XRD showed that the sharp peaks of the crystalline structure are lost due to the substitution of the organic linker by phosphate which collapses the crystalline structure. Various solutions of chemicals that nanocarriers can encounter in human bodies such as reactive oxygen species H_2O_2, H_4PDP and phosphate were exposed to both coated and uncoated MOFs. Uncoated MOFs showed no color change in solutions compared to uncoated MOFs that exhibited a change in color, thus indicated undesirable reactions, establishing the sealing ability and impermeability of the lipid bilayer, Figure 10.

Cellular uptake of coated MOFs and uncoated MOFs was experimented by HeLa and SMMC-7721 cells, respectively. A rapid release of the red fluorescence dye from uncoated MOFs compared to coated ones showed a higher uptake by both cell lines and no release was observed [65].

Figure 10: The corresponding photographs illustrating the changes of bare and coated nano Zr MOFs suspensions under various chemical environments (100 mM) or 10% of the above compounds [62].

Juewen Liu et al. studied liposomes fusion with silica nanoparticles using the electrical charges difference as the driving force for fusion. Cationic silica nanoparticles loaded with calcein were coated with negative and positive liposomes, and cellular uptake experiments were the prime indicator of the successful fusion. Negatively charged liposomes from DOPS (1,2- dioleoyl-sn-glycero-3-phospho-L-serine) were prepared using the hydrating method and simple incubation with the loaded silica particles for 45 minutes with occasional agitating by manual pipetting resulted in coated particles.

Cellular uptake experiments by Chinese hamster ovary (CHO) cells showed a moderate improvement compared to uncoated silica particles, however, the retention of calcein within the silica particles improved by ∼55% indicating charge repulsion. Further charge modification of negatively charged liposomes by mixing with positively charged liposomes using DOTAP (N- [1-(2, 3-Dioleoyloxy) propyl]-N, N, N-trimethylammonium methyl-sulfate) and the same procedure for coating, showed a reduction in calcein release by ∼75% and the remarkable improvement in the cellular

33

uptake by CHO cells. Further confirmation of the fusion was established using fluorescence confocal microscopy (FCM) (Figure 11) and TEM [66].
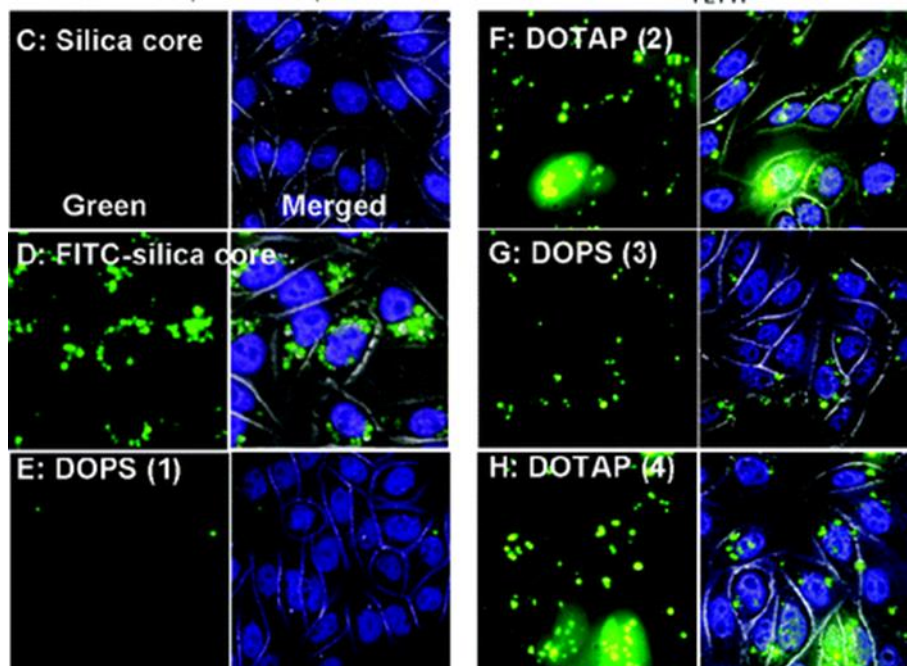
Figure 11: Fluorescence microscopy studies of CHO cells incubated with calcein-loaded cationic silica core or protocells after successive lipid fusion/exchange with oppositely charged liposomes. Stronger green emission indicates a higher level of calcein delivery [63].

Jin-Ho et al. improved the colloidal stability of gold nanoparticles by synthesizing nanogold particles inside liposomes. DSPC (2-distearoyl-sn-glycero-3-phosphocholine) liposomes-encapsulating the reduction agents were redispersed in solutions of the metal precursor. The metals diffused into the liposomes core and went through the reduction of the reactions that resulted in a self-crystalline of metal nanoparticles inside the liposomes. According to the metal precursor type (that is, Au, Ag, Pd, Pt, Au-Ag, Au-Pd, and Au-Pt precursors), various gold nanoparticles were synthesized. The confirmation of the coated synthesized nanoparticles was established using TEM images and UV−vis spectra for controlled samples of liposomes with and without the reducing agents, since a change in color was observed for reducing agents loaded liposomes only. The colloidal stability of these hybrids was investigated by the incubation with various biological solutions that showed the effectiveness of the lipid layer in preventing undesired interactions compared to uncoated particles. Furthermore, cellular uptake experiments by Homo sapiens brain glioblastoma U-87 MG cells

supported an improved efficiency of endocytosis of the hybrid nanoparticles with ten times greater improvement than uncoated gold nano particles [67].

2.5.   Ultrasound in Triggering Release

The challenge in any nano-drug delivery system is having an extended circulation yet is destabilizing at the encounter of cancer cells. Various triggers have been utilized and studied to trigger liposomes in specific as they are the most used nanocarrier in the market compared to other carriers. Tumor-specific characteristics such as the pH and overexpression of certain enzymes are among the attributes that have been utilized to promote the release of drugs. In addition, thermo sensitivity triggering is achieved using UV, visible light and NIR wavelengths. However, some of those tactics can induce undesired side effects. For example, using UV, biomolecules can absorb UV-light which may lead to the destruction of the agent making, which makes it a less suitable trigger [68]. Ultrasound (US) triggering is one of the most triggering techniques. It has been used to enhance the delivery and activity of drugs for the past two decades [69]. It consists of sound waves at frequencies above those within the hearing range of the average person (>20 kHz). US waves are unique as they can induce a physical movement within molecules and cells. They compress at high pressures and expand at low pressures [70]. Also, US waves like other wave carry energy that can be absorbed by the medium. Thus, they can transmit energy.

The dual mechanical and thermal effects that US waves can induce in tissues lead to usage in effectively controlling the drug release from liposomes. The thermal effect (hyperthermia) of US waves employs the carried energy by the waves to heat the tissues, thus disrupting the liposomes membranes as the bilayer transitions from ordered gel phase to liquid crystalline phase and free volumes within the bilayer to enable the drug to move across the lipid bilayer [70].The physical mechanism of ultrasound in triggering the breakup of liposomes is acoustic cavitation. The growth, oscillation and collapse of the small formed bubbles near the interfaces of liposomes induce high shear stresses that can eventually rupture the phosphor-bilayers [71].

MOFs release triggering methods have not been researched, thus researchers have depended mainly on simple diffusion to release the drug as the main concern was the minimum cellular uptake of MOFs as a prime obstacle that needs to be addressed first.

Chapter 3. Objectives

The objective of this thesis is to develop a successful drug delivery nanocarrier from incorporating liposomes and MOFs that can overcome the limitations of the liposomes and MOFs as individual drug carriers. The following goals were set to meet the objectives:

- To prepare PEGylated liposomes using the thin-film hydration method.

- To characterize-BTC MOFs using TEM, XRD, FTIR and TGA.

- To load Fe-BTC MOFs with Calcein as a model drug.

- To evaluate the efficiency of MOFs-loading using spectrofluorometry.

- To encapsulate MOFs using liposomes while maintaining the loading efficiency of the MOFs.

- To Investigate the encapsulation of MOFs within the liposomes using several techniques including dynamic light scattering (DLS), and Zeta potential.

- To conduct and compare the release profiles of the hybrid Liposomes-MOFs systems with and without ultrasound as an external triggering mechanism.

- To model the ultrasound-assisted release of the agent using applicable mathematical kinetic models.

Chapter 4. Experimental Procedures

4.1. Materials

4.1.1. Liposomes. This 1,2-dipalmitoyl-sn-glycerol-3-phosphocholine (DPPC) and 1,2-distearoylsn-glycero-3- phosphoethanolamine-N-[amino(polyethylene glycol)-2000] (DSPEPEG2000-NH$_2$), the Avanti Mini Extruder extrusion kit were purchased from Avanti Polar Lipids Inc. (Alabaster, AL, USA). Potassium chloride (KCl) was obtained from (Unichem Laboratories Ltd., Mumbai, India). Monopotassium phosphate (KH$_2$PO$_4$) was obtained from BDH Laboratory Supplies (Poole, England, UK). Disodium phosphate (Na$_2$HPO$_4$) and disodium tetraborate decahydrate (Na2[B4O$_5$(OH)$_4$]). 8H$_2$O) were purchased from VWR International (Radnor, PA, USA). Sodium chloride (NaCl) was obtained from Merck Millipore (Burlington, MA, USA). The 0.2-µm polycarbonate membranes and filter support were obtained from Whatman PLC (Maidstone, England, UK). Chloroform (CHCl$_3$), and Cholesterol was obtained from Alfa Aesar (Ward Hill, MA, USA).

4.1.2. MOFs. Fe-BTC MOFs were obtained from Sigma-Aldrich (St. Louis, MO, USA) under the trade name Basolite F300. Calcein disodium salt (C$_{30}$ H$_{24}$ N$_2$Na$_2$O$_{13}$) was obtained from Sigma- Aldrich (St. Louis, MO, USA) through Honeywell Fluka. All chemicals were used as purchased without further modifications.

4.2. Methods

4.2.1. Characterization of Fe-BTC MOFs. Several characterization tests were conducted on FE-BTC MOFs such as TEM, TGA, FTIR and XRD. This section will discuss the characterization techniques used in this work.

- Transmission electron microscopy (TEM)

The morphology of the MOFs in terms of shape and size was investigated using TEM. Fe-BTC MOFs were magnified at around 187000X magnification. It was possible to capture the image within 268 ms.

- Thermogravimertic Analysis (TGA)

The thermal stability of Fe-BTC MOFs was investigated by measuring the changes in weight of a sample due to the effect increasing temperature, which indicated the rate of decomposition. The device used was a thermogravimetric analyser (TGA) (PerkinElmer, USA) in the chemistry department at AUS.

- Fourier-transform infrared spectroscopy (FTIR)

Fourier Transform Infrared Spectroscopy (FTIR) recognizes chemical bonds in a molecule by producing an infrared absorption spectrum that is distinct for every chemical bond. The FTIR produces a distinctive molecular profile similar to a fingerprint; it can be used to identify samples by comparing many different chemical bonds and components. The device used was a Fourier transform infrared spectroscopy (PerkinElmer, USA) in the chemistry department at AUS.

- X-ray diffraction pattern (XRD)

XRD is a technique used to determine the crystal structure of porous materials. The X-rays beam directed into the sample will diffract causing a pattern of high and low intensities. The range of diffraction peaks determines the crystal structure. Crystals peaks are very specific and sharp while amorphous materials show scattered patterns of broad rounded peaks.

4.2.2. Loading of Fe-BTC MOFs with calcein. A calcein solution of 0.3 mM was prepared by mixing 2.0 mg of calcein in 10.0 ml of distilled water at pH = 12. The solution was mixed using a Vortex mixer. 10.0 mg of Fe–BTC MOFs were further added to the calcein solution and left stirring at room temperature for 24 hours using a magnetic stirring plate. The resulting mixture was then centrifuged at 4000 rpm for 20 minutes. The supernatant was removed and the loaded MOFs were collected and dried in an oven at 100°C for one hour.

For measuring the loading efficiency of calcein for Fe-BTC MOFs, the fluorescence of calcein solution was measured before and after loading using fluorescence spectroscopy (QuantaMaster QM 30, Photon Technology International, USA) connected to FelixGX software with the emission wavelength set between 490 and 515 nm. The following calcein quantifying procedure was followed.100μL of the stock calcein solution was diluted in 2.5 ml distilled water at a pH = 12 and the fluorescence was measured and indicated as the initial fluorescence intensity (F1). After centrifuging the loaded MOFs, the supernatant fluorescence was measured following the same previous dilution (F2). The loading efficiency was calculated using the following equation.

$$Loading\ efficiency\ = \frac{F1-F2}{F1} \tag{1}$$

Where F_1 is the fluorescence of the model drug solution (before the loading), F_2 is the fluorescence of the supernatant after the loading.

4.2.3. Preparation of pegylated liposomes. The film hydration method was used to synthesize the liposomes, in a 250 ml-round flask, 19.2 mg of 1,2-dipalmitoyl-sn-glycerol-3-phosphocholine (DPPC), 4.7 mg of cholesterol and 5.58 mg DSPEPEG2000-NH$_2$ were dissolved in 4 ml chloroform. The chloroform solvent was evaporated using a vacuum that uses a rotary evaporator at 50°C for 15 minutes. Upon establishing the dry lipid film by inspection, a hydrating solution of 2 ml of PBS buffer was added and left to mix at 60°C for 50 minutes. The liposomes solution was then sonicated using a sonication bath at 40- kHz for 2 minutes at 60°C.The liposomal solution was further extruded at 60°C using 0.2-µm polycarbonate filters for 31 times.

4.2.4. Encapsulation of MOFs by liposomes. After the extrusion of the liposomes, the extruded solution was added to 1.5 mg of loaded Fe-BTC MOFs in a plastic tube and left for incubation at room temperature for 24 hours.

4.2.5. Confirming the encapsulation of Fe-BTC by dynamic light scattering . Zetasizer Nano Zs instrument (Malvern Instruments Ltd, UK) at University of Sharjah was used to determine the mean diameter of liposomes and coated Fe-BTC MOFs at 25 °C. The hydrodynamic diameter, polydispersity percentage (Pd%) and the cross-correlation patterns of the DLS signals were the criteria used to determine the average diameter of liposomes and coated Fe-BTC MOFs after the encapsulation.1 mL of liposomes was mixed with 1 mL of distilled water, and a sample was taken for measurements. For coated Fe-BTC MOFs, the same dilution procedure was followed, however, before taking a sample for measurements, the resulting solution was further centrifuged at 4500 rpm for 10 minutes to ensure that the DLS sample will represent the coated MOFs and not the free-roaming liposomes that may have not coated the Fe-BTC MOFs.

4.2.6. Encapsulation of MOFs by liposomes. Zetasizer Nano Zs instrument (Malvern Instruments Ltd, UK) at University of Sharjah was used to determine the electrical surface charge of unloaded Fe-BTC MOFs, loaded Fe-BTC MOFs and coated Fe-BTC MOFs at 25 °C. 1 ml was taken from a solution that is made from 1.5 mg of Fe-BTC MOFs in 1 ml PBS. It was further mixed with another 1 ml of distilled water. A sample was taken for measurements and the same procedure was followed for loaded Fe-BTC MOFs. In the coated Fe-BTC MOFs, 1 ml solution of them was mixed with 1 mL of distilled water then the resulting solution was further centrifuged at 4500 rpm

for 10 minutes to ensure that the zeta potential measurements indicate the coated MOFs and not the free-roaming liposomes that may have not coated the Fe-BTC MOFs.

4.2.7. Confirming the encapsulation of Fe-BTC by cryo-TEM. Cryo-TEM imaging using NANOSPRT5 at the University of Western Ontario (Canada), was used to measure the size of loaded and coated MOFs to further determine the difference in the diameter of these proposed nanocarrires, after encapsulation. 1 ml solution of the coated and loaded MOFs was magnified at around 187000X magnification. It was possible to capture the image within 268 ms.

4.2.8. Investigating the encapsulation of Fe-BTC by release experiments without the use of ultrasound. To further investigate the effectiveness of the MOFs encapsulation, calcein release was investigated; mainly to investigate the effect of incubation to prevent the premature release of the MOFs due to diffusion. Release experiments were conducted on loaded Fe-BTC MOFs and coated loaded Fe-BTC MOFs. 1.5 mg of the loaded MOFs was added to 1 ml PBS solution and was further mixed with 14 mL distilled water at a pH of 12. In the coated Fe-BTC MOFs, since during the incubation was with 1 ml of liposomes solution, only 14 mL of distilled water at pH = 12 was added and the resulting solution. Distilled water at pH = 12 was used as the releasing medium because of the self-quenching properties of Fe-BTC MOFs with calcein. At pH = 7, calcein tends to bond with iron at the iminodiacetic arms, thus quenching the model drug's fluorescence [72]. Tenopoulou, Margarita et al. argued that the iron calcein bind is pH specific, hence, a change in pH (to a more alkaline medium) can cause the iron to detach from the calcein, thus regaining its characteristic fluorescence [73].The resulting solutions were poured into plastic tubes, then were incubated in a water bath at $37 \pm 0°C$. A baseline was established by measuring the fluorescence of the mixture before incubating it in the water bath. The release procedure was repeated at several times increments. In each round, the samples were centrifuged at 1500 rpm for two minutes to ensure that the measured fluorescence was from the calcein released from the MOFs pores, not the one that may have remained on the surface of the MOFs after loading. Then 3 ml of the resultant solution were taken into a cuvette, and the fluorescence was measured. The same procedure was repeated at time increments of 5, 10, and 20 minutes.

4.3. Statistical Analysis

A standard t-Test was conducted to compare several parameters; namely the effect of ultrasound on drug release and the effect of the liposomal coating on calcein release. A two-tailed t-test with confidence level of 95% ($\alpha = 0.05$) was chosen.

4.4. Mathematical Modelling

For the application of nanocarriers in therapeutic drug delivery, several parameters govern their future utilization in clinics, including, biocompatibility, circulation time and release profiles. These guidelines serve as the foundation for utilizing nanocarriers in the drug delivery, namely in cancer treatment. The knowledge of the exact mass of the drug being released at each time increment is an important parameter that needs to be investigated in the treatment of cancer. A high drug dose can cause severe side effects such as cardiotoxicity [74]. Equally, a low drug release may hinder the efficiency of the treatment and allow the cancer cells to develop multi-drug resistance. Notably, the cancer to be treated is sensitive to the amount of the drug delivered. For example, in a study it was reported that a high dose of chemotherapy drugs caused more reduction in cancer cells in lymphoma cancer in contrast to breast cancer, in which the dose of the drug does not affect the rate of reduction in cancer cells [75] .

Several mathematical models have been developed to explain the dissolution of the drug and can be utilized to predict the drug release. Additionally, providing the right mathematical model can determine factors that affect drug release. Accordingly, this section will discuss several mathematical drug release models; namely, zero-order, first-order, Higuchi, Kormeyers Peppas, Baker Lonsdale, Hixson, Weibull, Hopfenberg and Gompertz. The models will be explained in terms of the concept behind them and the mathematical equations for each model.

4.4.1. Zero order. This model assumes that the drug release is a function of time only, which is mainly found in the case of a very slow drug release [76]. The following equation represents this model:

$$Q_0 - Q_t = k_0 t \tag{2}$$

In which Q_t is the amount of drug released at time t, Q_0 is the initial amount of drug in the solution at $t = 0$, (typically, $Q_0 = 0$) and k_0 is the zero-order release constant expressed in units of concentration per time. By modifying this equation by the cumulative release percentage (*CFR*), which is

41

$$CFR = \frac{Drug\ released\ at\ any\ time, t - Initial\ Amount}{Total\ amount\ of\ drug\ present} = \frac{Q_t - Q_0}{Q_T} \tag{3}$$

we get the following equation:

$$CFR = k_0 t \tag{4}$$

A plot of *CFR vs. t* gives a straight line with a slope of k_0.

4.4.2. First order. This model links the drug release rate with the concentration gradient between the drug carrier and the bulk fluid adjacent to it. Hence the higher the concentration gradient, the higher the drug release [77]. The following equation is used to model this behavior:

$$\frac{dC}{dt} = -kC \tag{5}$$

In which, C is the percent of the drug remaining at time t and k is the first-order rate constant, expressed in time^{-1}. The previous equation can be further expressed in the following form:

$$ln(C) = ln(C_0) - kt \tag{6}$$

Where C is the total amount of the drug that remain and C_0 is the initial amount of drug. In terms of CFR, the equation becomes:

$$ln(1 - CFR) = -kt \tag{7}$$

A plot of ln(*1-CFR*) *vs.* time should give a straight line with a slope of k.

4.4.3. Higuchi. This is the first model used to describe drug release from a matrix system. It was based on the following hypotheses:

- The initial drug concentration in the matrix is much higher than drug solubility.
- Drug diffusion takes place only in one-dimension and is constant.
- The drug particles are much smaller than system thickness.
- The matrix swelling and dissolution are negligible.
- Perfect sink conditions are always attained in the release environment.

Consequently, the following mathematical model is derived:

$$Q = A\sqrt{DC_s(2C_0 - C_s)t} \tag{8}$$

where Q is the cumulative amount of the drug released in time t per unit area, C_0 is the initial drug concentration, C_s is the drug solubility in the matrix, and D is the diffusion coefficient of the drug molecule in the matrix [77]. The model is further simplified into:

$$Q = k_h\sqrt{t} \tag{9}$$

In which k_h, is the Higuchi dissolution constant.

The model can be expressed in terms of *CFR* as follows:

$$CFR = \frac{k_h\sqrt{t}}{Q_T} - \frac{Q_0}{Q_T} \tag{10}$$

A plot of *CFR* vs. $\sqrt{t}$ should give a straight line with a slope of $\frac{k_h}{Q_T}$, where Q_t represents the total amount of the drug available.

4.4.4. Korsmeyers Peppas.

This model is integrated based on the concept that the drug release is due to diffusion. It provides a definition of the type of diffusion that is responsible for drug release. The following equation is used to represent the model:

$$\frac{M_T}{M_\infty} = k\,t^n \tag{11}$$

Where $\frac{M_T}{M_\infty}$ is a fraction of drug released at time *t*, *k* is the release rate constant and *n* is the release exponent. The *n* value is used to characterize different release mechanisms such as Fickian diffusion and erosion mechanism. The equation can be further simplified in terms of *CFR* to yield:

$$CFR \approx kt^n \tag{12}$$

The linearized form of the above equation is as follows:

$$log(CFR) = log(k) + n\,log(t) \tag{13}$$

A plot of log (*CFR*) *vs* log(*t*) should give a straight line with a slope of *n* and *y*-intercept of log (*k*).

4.4.5. Hixson Crowell.

This model studies the drug release with a changing surface area of the particles or tablets:

$$W_0{}^{1/3} - W_t{}^{1/3} = k\,t \tag{14}$$

Where W_0 is the initial amount of drug, W_t is the remaining amount of drug and k is the Hixson-Crowell constant describing the surface volume relation.

The equation can be further written in terms of *CFR* as follows:

$$(1 - CFR)^{1/3} = k\,t \tag{15}$$

A plot of the cube root of *1 – CFR* versus time gives a straight line with slope of *k*.

4.4.6. Weibull.

This model is widely used for the drug release and dissolution analysis. The parameters of this model lacks any physical parameters or a kinetic basis, hence it has been criticized because it does not represent a physical system [78]. The mathematical equation that represents this model is:

$$M = M_0\left(1 - e^{-\frac{(t-T)^b}{a}}\right) \tag{16}$$

Where M is the amount of drug as a function of time t, M_0 is total amount of drug being released, T accounts for the lag time measured as a result of the release process, a is a scale parameter that describes the time dependence, and b describes the shape of the release curve. For $b = 1$, the shape of the curve corresponds to the shape of an exponential profile with the constant $k = 1/a$. If $b > 1$, the shape of the curve gets sigmoidal, whereas the shape of the curve with b < 1 would show a steeper increase than the one with $b = 1$ [77].

In terms of CFR, the corresponding Weibull equation is:

$$\log(-\ln(1 - CFR)) = -\log(k') + b \, log(t) \tag{17}$$

Where k' is -T/a and b is 1/a.

A plot of $\log(-\ln(1 - CFR))$ *vs.* $log(t)$ gives a straight line with a slope of b.

4.4.7. Hopfenberg. This model relates the surface shape of the drug carrier to the release rate. It is based on the hypothesis that the surface remains constant as the dissolution process takes place [79]. It is represented by the following equation

$$\frac{M_t}{M_\infty} = 1 - \left[1 - \frac{k_0 t}{C_l a_0}\right]^n \tag{18}$$

Where $\frac{M_T}{M_\infty}$ is a fraction of drug released at time t, k_0 is the surface erosion rate constant, C_l is the initial drug concentration of the drug in the matrix, a_0 is the drug carrier half thickness (i.e. the radius for a sphere or cylinder), and n is an exponent that varies with geometry $n = 1$, 2 and 3 for flat, cylindrical and spherical geometry, respectively.

The equation can be further written in terms of *CFR* as follows:

$$1 - (1 - CFR)^{\frac{1}{3}} = k_{Hf} \, t \tag{18}$$

Where $k_{Hf} = \frac{k_0}{C_l a_0}$, n was chosen as 3 since both MOFs and liposomes are of spherical in shape. A graph between $1 - (1 - CFR)^{\frac{1}{3}}$ *vs* time should give a straight line with a slope of k_{Hf}.

4.4.8. Gompertz. This model is used for the comparative analysis of the intermediate drug release rate with good solubility [79]. It is represented by the following equation:

$$X(t) = X_{max} \exp\left[-\alpha e^{\beta \, log(t)}\right] \tag{20}$$

where *X(t)* = percent dissolved at time *t*; *Xmax* = maximum dissolution; α is described as location or scale parameter which determines the undissolved proportion at time $t =$

1 and β is the dissolution rate per unit of time and is often described as a shape parameter. The equation can be further written in terms of *CFR* as follows:

$$ln(-\ln(CFR)) = \beta \log(t) + \ln(\alpha) \tag{21}$$

A plot of $\ln(-\ln(CFR))$ *vs.* $\log(t)$ gives a straight line with a slope of k.

4.4.9. Baker Lonsdale. This model is based on the Higuchi model with the assumption that the matrix is spherically shaped [79]. This model can be represented by the following equation:

$$\frac{3}{2}\left[1 - \left(1 - \frac{M_t}{M_\infty}\right)^{\frac{2}{3}}\right] - \frac{M_t}{M_\infty} = kt \tag{22}$$

where the release rate constant, k, corresponds to the slope.

The equation can be further written in terms of *CFR* as follows:

$$\frac{3}{2}\left[1 - (1 - CFR)^{2/3}\right] - CFR = kt \tag{23}$$

A plot of $\frac{3}{2}\left[1 - (1 - CFR)^{2/3}\right] - CFR$ *vs.* t should give a straight line with a slope of k. A summary of all the drug release models, in terms of *CFR*, is presented in Table 3.

Table 3: Summary of the drug release kinetics models.

Model	Linearized equation	Parameters	Release mechanism
Zero Order	$CFR = k_0 t$	Slope $=k_0$	Diffusion mechanism
First order	$\ln(1 - CFR) = -kt$	Slope $=k_0$	Diffusion mechanism
Higuchi	$CFR = \dfrac{k_h\sqrt{t}}{Q_T} - \dfrac{Q_0}{Q_T}$	Slope $=\dfrac{k_h}{Q_T}$ Intercept $=\dfrac{Q_0}{Q_T}$	Diffusion mechanism
Korsmeyers Peppas.	$\log(CFR) = \log(k)$ $+ n \log(t)$	Slope $=n$ Intercept$=\log(k)$	Diffusion mechanism Semi-empirical
Baker Lonsdale	$\dfrac{3}{2}\left[1 - (1 - CFR)^{2/3}\right]$ $- CFR = kt$	Slope $=k$	Diffusion mechanism
Hixson Crowell	$(1 - CFR)^{1/3} = k\,t$	Slope $=k$	Erosion mechanism
Weibull	$\log(-\ln(1 - CFR))$ $= -\log(k') + b \log(t)$	Slope $=b$ Intercept$=\log(k)$	Empirical model, life-time distribution function.
Hopfenberg	$1 - (1 - CFR)^{\frac{1}{3}} = k_{Hf}t$	Slope $=k_{Hf}$	Erosion mechanism
Gompertz	$\ln(-\ln(CFR))$ $= \beta \log(t)$ $+ \ln(\alpha)$	Slope $= \beta$ Intercept$=\ln(\alpha)$	Dissolution mechanism

Chapter 5. Results

5.1. Characterization of Fe-BTC MOFs

5.1.1. TEM images of Fe-BTC MOFs. The TEM image shows that the morphology of Fe-BTC MOFs is irregular with an average diameter of 100 nm as shown in Figure 12, which is consistent with data reported in literature [80].
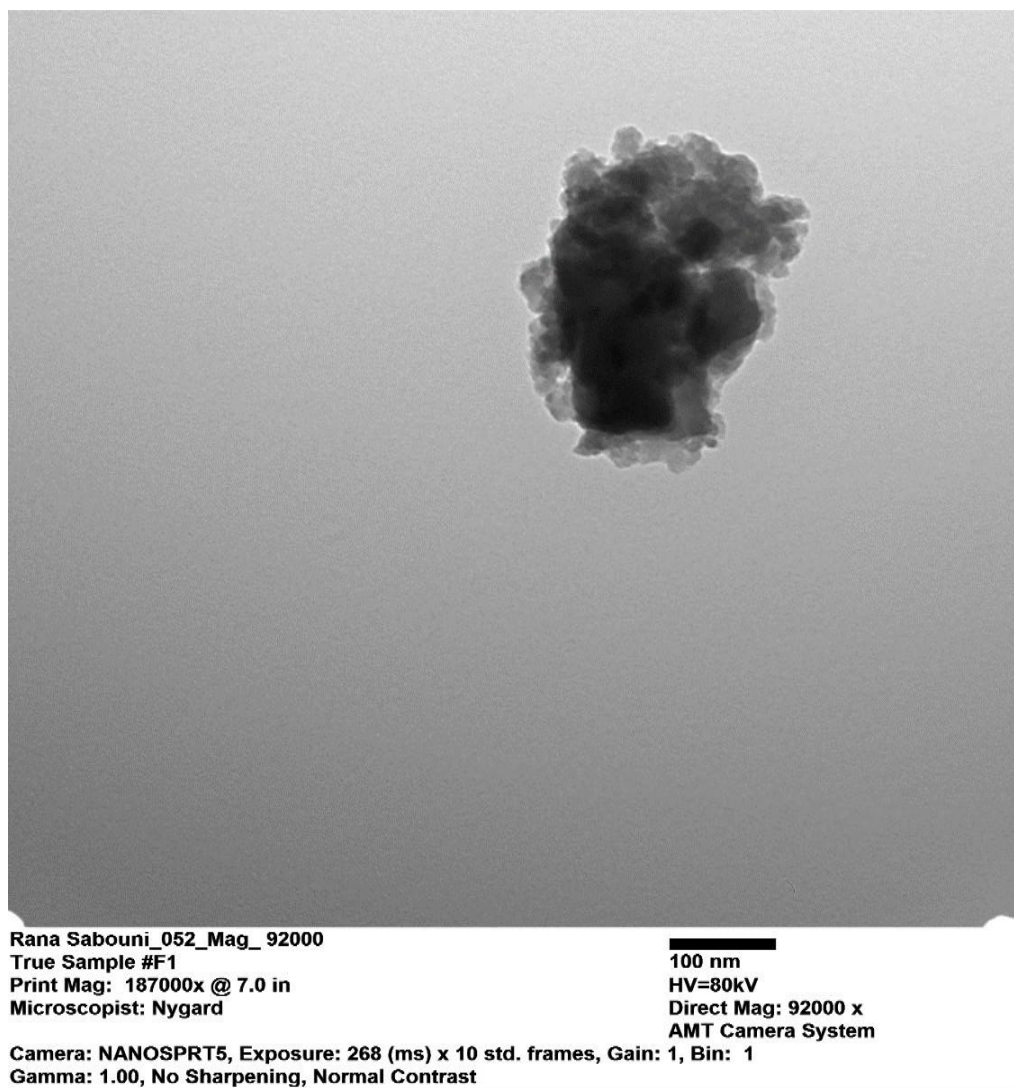
Rana Sabouni_052_Mag_ 92000
True Sample #F1
Print Mag: 187000x @ 7.0 in
Microscopist: Nygard

100 nm
HV=80kV
Direct Mag: 92000 x
AMT Camera System

Camera: NANOSPRT5, Exposure: 268 (ms) x 10 std. frames, Gain: 1, Bin: 1
Gamma: 1.00, No Sharpening, Normal Contrast

Figure 12: TEM images of Fe-BTC MOFs.

5.1.2. XRD pattern of Fe-BTC MOFs. Figure 13 represents the XRD patterns of Fe-BTC. According to the XRD spectrum, Fe-BTC has a crystalline porous structure with distinctive sharp diffraction peaks. This is consistent with previous findings in literature [80].
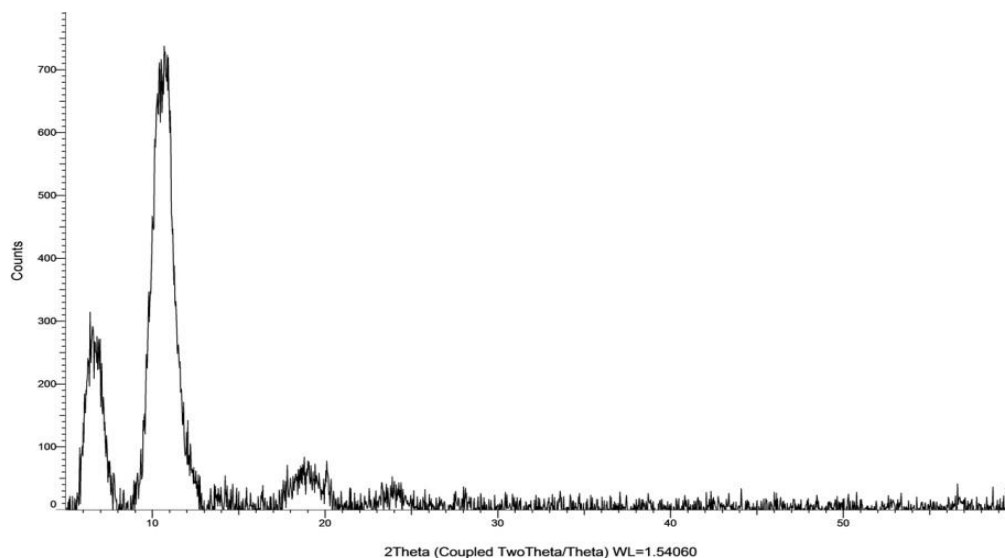
46

Figure 13: XRD pattern of Fe-BTC MOFs.

5.1.3. TGA analysis of Fe-BTC MOFs. The TGA result shows that the Fe-BTC MOFs undergo a thermal single stage degradation beginning at 400˚C and with a total mass loss of 94.5% as shown in Figure 14. The mass lost before 100 ˚C is due to the loss of moisture associated with the sample as reported in literature [81].
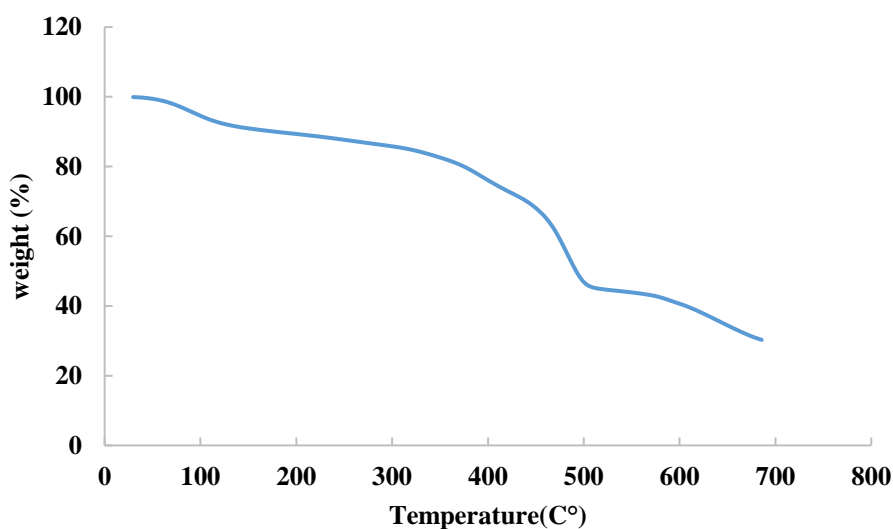

Figure 14: TGA of Fe-BTC MOFs.

5.1.4. FTIR of Fe –BTC MOFs. The infrared absorption spectrum of Fe-BTC MOFs was found consistent with literature [82]. It can be divided into two zones: one representing the bond between the iron and trimesic acid and the other represents the trimeric acid, Figure 15. The vibrations at 500 $cm-1$ represent the Fe-O bonds, followed by several vibrations representing the trimesic acid. The zone at 750 $cm-1$

47

represents the C-H bonds stretching of the benzene ring. At around 1250 $cm-1$ there are C-O bonds stretching, followed by the vibration of O-H bonds at 1500 $cm-1$ and stretching of C=O at 1750 $cm-1$.The final stretching of O-H bonds is at 3200 $cm-1$.
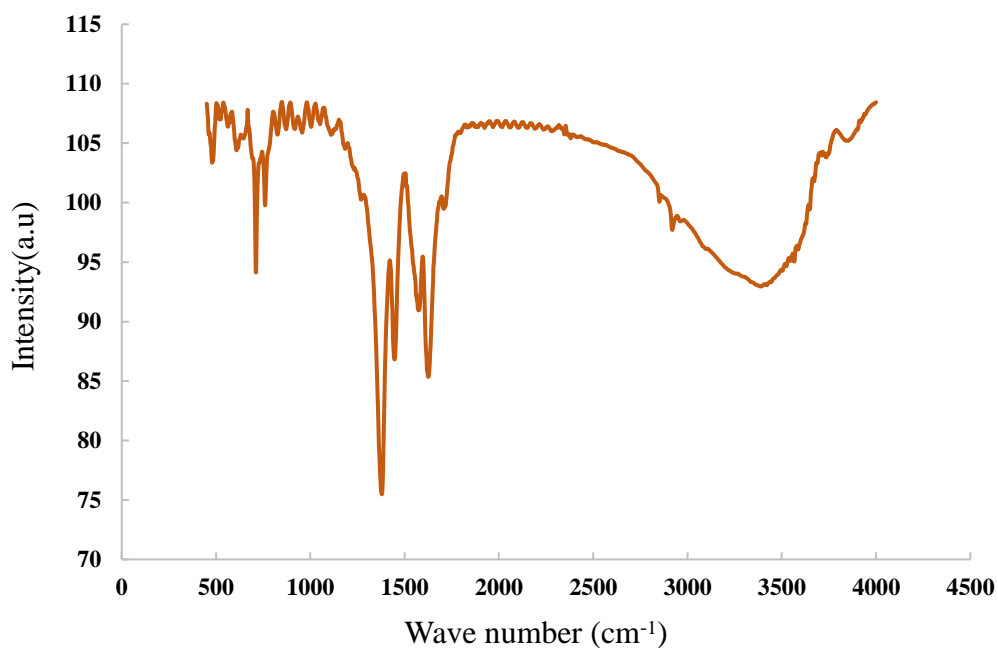

Figure 15: FTIR of Fe-BTC MOFs.

5.2. Loading Efficiency of Fe-BTC MOFs

The loading efficiency of calcein in Fe-BTC MOFs was calculated using equation (1) and was found to be 17.37% on average with a standard deviation of 0.54. This relatively low efficiency could be primarily because the pores of Fe-BTC MOFs are slightly hydrophobic compared to their hydrophilic surface. Table 4 summarizes the loading efficiency for three trials.

Table 4: Fluorescence intensity of the mother calcine solution and the supernatant.

Trial	F1	F2	Loading efficiency %
1	32.19	26.39	18.00
2	32.19	26.71	17.02
3	32.19	26.68	17.11

5.3. DLS Results of Liposomes and Coated Fe-BTC MOFs

Table 5 summarizes the radius changes in coated Fe-BTC MOFs and liposomes from three different batches. The results showed a radius increase by 12-14.6 nm which is acceptable since the coated Fe-BTC is still under 200 nm, which is one of the main concerns of nano-drug carriers. Larger-sized nanoparticles can trigger and activate the immune system, hence they will get cleared before reaching the cancer site [83].

Table 5: Radius measurements of Fe-BTC MOFs before and after encapsulation.

Trial	Liposomes		Coated Fe-BTC	
	Diameter(nm)	Polydispersity (Pd) %	Diameter (nm)	Polydispersity (Pd) %
1	150.9	16.0	165.5	12.5
2	149.3	14.8	161.3	11.8
3	149.8	16.9	162.5	9.0
Average	150±0.82		163.1±2.16	

Figure 42 and Figure 43 in the appendix show the intensity weighted particle size distribution, while Figure 44 and Figure 45 show the cross-correlation signals of positive correlation indicating that the samples were stable during repetitive measurements.

5.4. Cryo-TEM Results of Uncoated and Coated Fe-BTC MOFs

To further verify the presence of the liposomal coating, Cryo-TEM images of the coated Fe-BTC MOFs were compared to the Cryo-TEM image of Fe-BTC MOF in terms of diameter. Figure 16 and Figure 17 show the Cryo-TEM images of coated and uncoated Fe-BTC MOFs. Using the obtained Cryo-TEM images, the diameters were calculated and are shown in Table 6.

Table 6: Radius measurements of Fe-BTC MOFs before and after encapsulation.

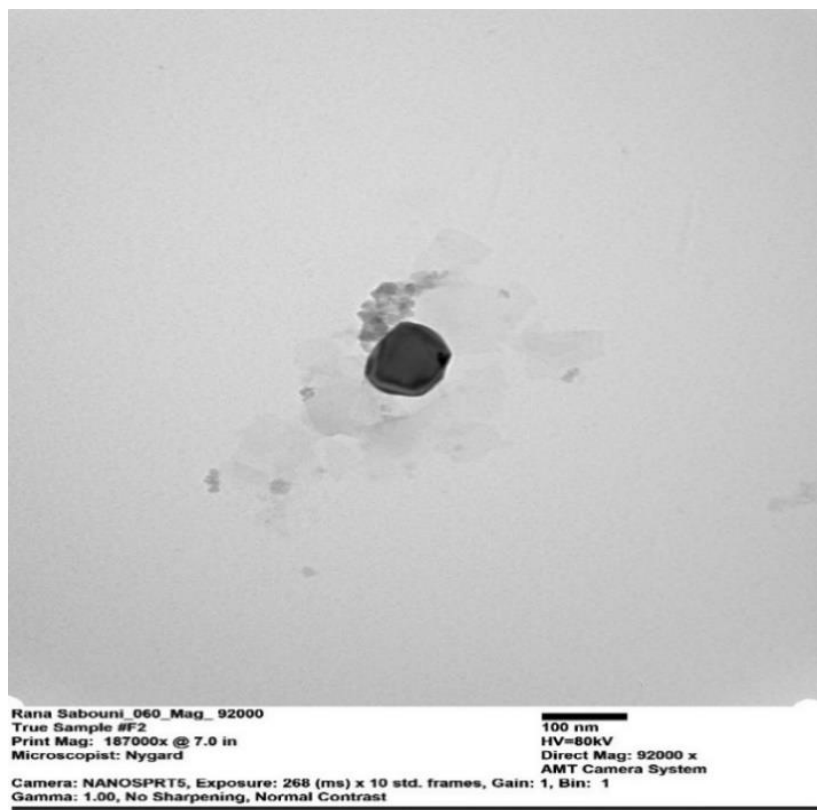| Fe-BTC MOFs Diameter(nm)	Coated Fe-BTC MOFs Diameter (nm)
155.55	169.23

Rana Sabouni_060_Mag_ 92000
True Sample #F2
Print Mag: 187000x @ 7.0 in
Microscopist: Nygard

100 nm
HV=80kV
Direct Mag: 92000 x
AMT Camera System

Camera: NANOSPRT5, Exposure: 268 (ms) x 10 std. frames, Gain: 1, Bin: 1
Gamma: 1.00, No Sharpening, Normal Contrast

Figure 16: Cryo-TEM image of Fe-BTC MOFs.

Coated MOF_010
Coated MOF-NonStained8
Print Mag: 130000x @ 7.0 in
12:08 1/24/2019
Microscopist: RKhazaee
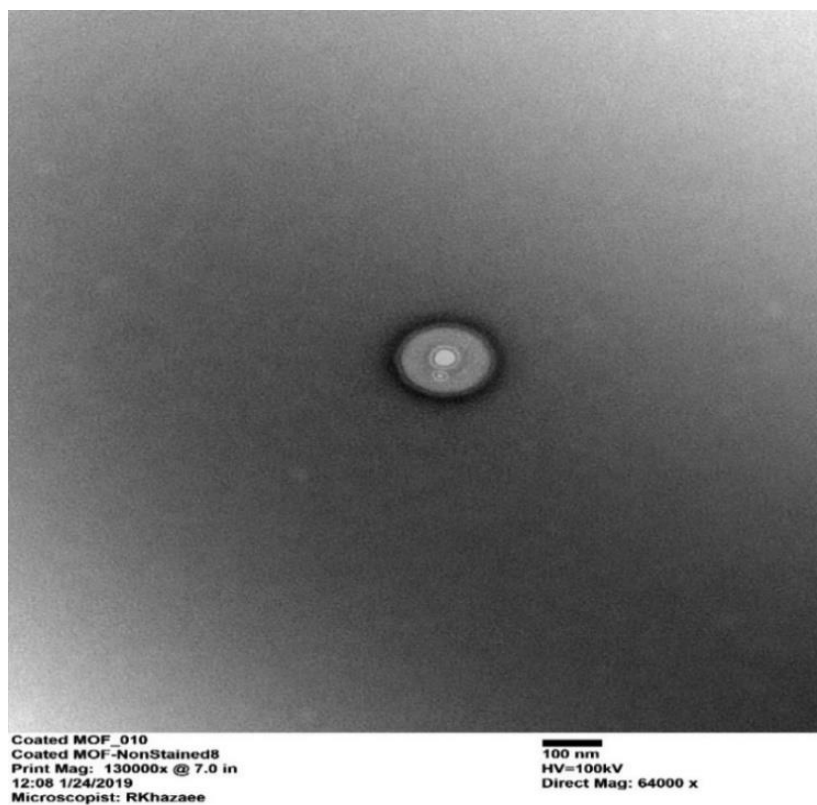
100 nm
HV=100kV
Direct Mag: 64000 x

Figure 17: Cryo-TEM image of coated Fe-BTC MOFs.

50

There is a difference of around 14 nm between the uncoated and coated MOFs, which is anticipated as the bilayer thickness is typically around 7.5-10 nm and the attachment of DSPEPEG2000-NH2 attributed to the extra change in the radius because it has a long polymeric chain [84]. The cryo-TEM measurements of the sample's diameters agree with the DLS measurements reported earlier.

5.5. Zeta Potential Results of Unloaded Fe-BTC MOFs, Loaded Fe-BTC MOFs and Loaded Coated Fe-BTC MOFs

The unloaded Fe-BTC MOFs showed a negative charge as shown in Table 7, which can be attributed to the COO^- group of the Trimesic acid in Fe-BTC MOFs. This result agrees with the literature [85]. The loaded Fe-BTC MOFs exhibited even a more negative charge due to the calcein encapsulation. Calcein has a net negative charge due to the unequal sharing of electrons from the oxygen atoms [86]. Hence, loaded Fe-BTC MOFs are more negatively charged as calcein diffuses into the pores. The coated Fe-BTC MOFs were found to be neutrally charged, due to the coating effect of the neutrally charged lipids used to synthesize the liposomes. This confirms the coating of the Fe-BTC MOFs. Previous studies have shown that neutrally charged MOFs can improve the circulation time of the nanocarrier. Cancer cells tend to have a negatively charge surface, thus a negatively charged drug carrier can be repelled due to electrostatic forces, lowering its efficacy [87]. Figure 46 and Figure 47 in the appendix show the charge distribution. The charge of the nanocarriers also gives an indication about the physical stability behavior .Loaded MOFs surface charge was significantly lower than -30 mV ,hence indicating good stability due to electrotactic repulsion .On contrast unloaded and coated MOFs showed low surface charges which indicate that they might agglomerate on the long term usage ,as Van der Waals attractive forces interact between nanoparticles when surface charge is between ±25mV [88] .

Table 7: Zeta potential values of Fe-BTC MOFs before and after encapsulation.

Trial	Unloaded Fe-BTC (mv)	Loaded Fe-BTC (mv)	Coated Loaded Fe-BTC (mv)
1	-14	-39	+6.76
2	-12.9	-39.8	+5.86
3	-12	-39.2	+6.07
Average	-12.97$\pm$1.00	-39.33$\pm$0.42	+6.23$\pm$0.47

5.6. Fluorescence Release Experiments

To determine the percentage of drug release at each time interval, the following equation was used:

$$Release\ (\%) = \frac{f_t - f_o}{f_m - f_o} \times 100 \tag{23}$$

Where

f_o is the fluorescence intensity at the baseline?

f_t is the fluorescence intensity at time (t) interval.

f_m is the intensity at maximum release.

To calculate the f_m, the usage of the loading efficiency was utilized to calculate the maximum concentration as follows:

Amount of drug encapsulated (mg) in 10 mg of MOFs = loading efficiency × concentration of the loading solution (mM)×calcein molecular weight (mg/mmol) × amount of the loading medium (10 ml).

Then, the amount of calcein in 1.5 mg of MOFs was calculated:

Amount of drug encapsulated(mg) in 1.5mg of MOFs= amount of drug encapsulated(mg)in 10 mg of MOFs × [(1.5 mg MOFs)/ (10 mg MOFs)]

To calculate the final maximum concentration was as follows:

Maximum concentration (mM)= (amount of drug encapsulated(mg) in 1.5 mg of MOFs) / [(calcein Molecular weight (mg/mmol) ×amount of the release solution medium)].

Table 8 shows the calculated maximum calcein concentrations achieved for three trials.

Table 8: Maximum calcein concentration (mM) calculated for three trials.

Trial	Loading efficiency %	Maximum concentration (mM)
1	18.00	5.40×10^{-3}
2	17.02	5.10×10^{-3}
3	17.11	5.133×10^{-3}
Average	17.37 ± 0.54	$5.211 \times 10^{-3} \pm 1.65 \times 10^{-4}$

A calcein calibration curve using distilled water at pH = 12 was established to calculate the released calcein concentrations at time t. Distilled water a pH 12 was used in the loading solution and as a release medium, thus it was used in the calibration curve. The calibration curve is shown below in Figure 18. Note: The fluorescent spectrum for the calibration curve is shown in the appendix ,Figure 48.
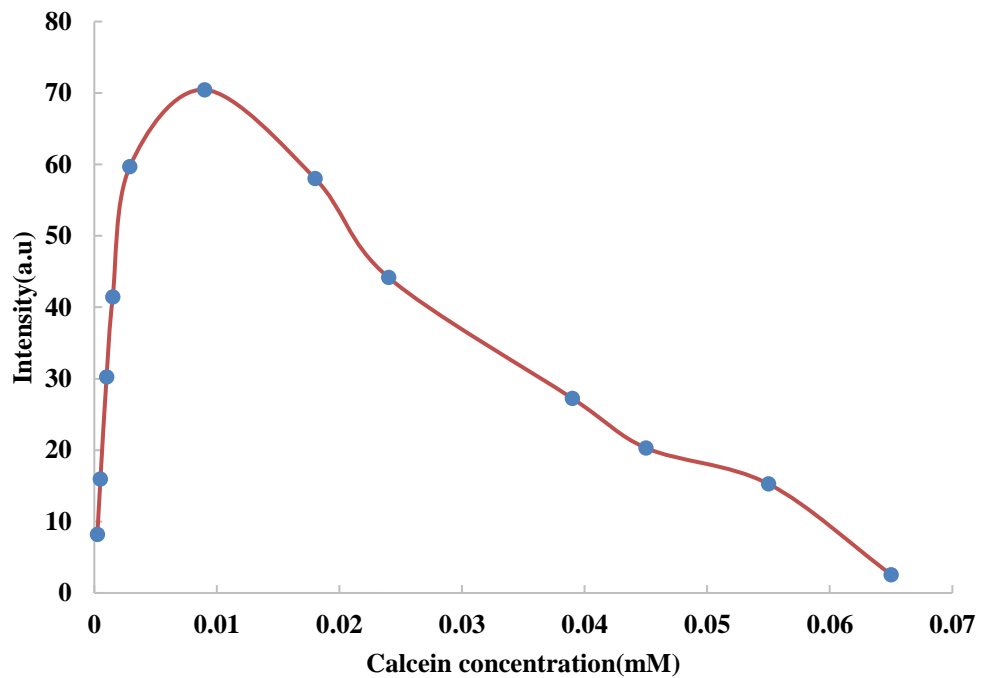

Figure 18: Calcein calibration curve.

As the average maximum concentration was 5.211×10^{-3} mM,which is in the non-self-quenching region. A mathematical equation that models the non-self-quenching region was defined using MATLAB (R2019 a) software. The following equation was chosen as the best fit of the non-self-quenching region with a coefficient of determination (R^2) of 0.99.

$$f = \frac{83.47x - 1.088 \times 10^{-2}}{1.26 \times 10^{-3} + x} \tag{24}$$

Where

f is the fluorescence intensity

x is the Calcein concertation in mM

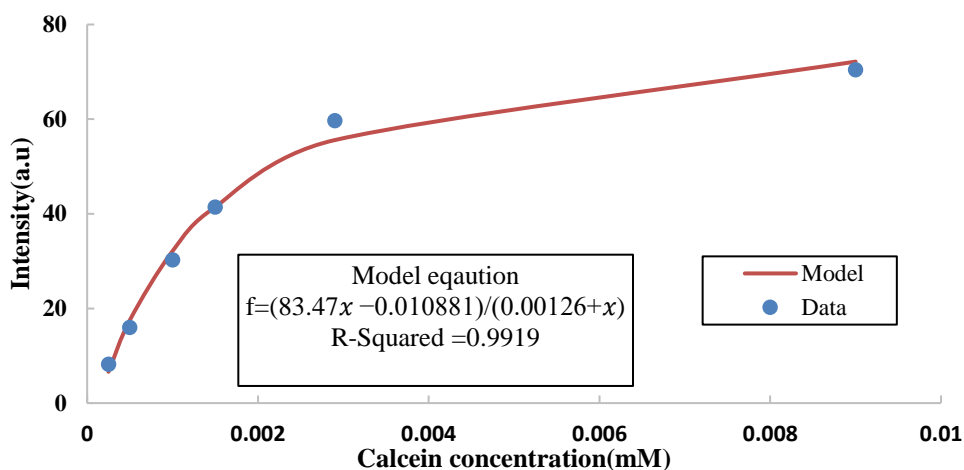Figure 19 shows the data points and the chosen model.

Figure 19: Calibration curve for Calcein model in the non-self-quenching region.

Based on the model, the fluorescence intensity for the maximum concentration was calculated, and Table 9 summarizes the results.

Table 9: Maximum calcein maximum fluorescence intensity calculated for three trials.

Trial	Maximum concentration (mM)	f_m
1	5.40×10^{-3}	66.04
2	5.10×10^{-3}	65.22
3	5.133×10^{-3}	65.32
Average	$5.211 \times 10^{-3} \pm 1.65 \times 10^{-4}$	65.53 ± 0.44

5.7. Release Experiments of Uncoated and Coated Fe-BTC MOFs Without Ultrasound

Controlled drug release experiments of the model drug calcein without the usage of ultrasound were conducted on uncoated Fe-BTC MOFs and coated Fe-BTC MOFs at the normal human body temperature of 37 °C using distilled water at pH = 12. Figure 20 compares the release profiles of both samples with three trials. The average of the trials is shown with standard deviation error bars. The graph shows that coated MOFs only reached around 1.2% release compared to uncoated MOFs that reached up to 4.3% within 70 minutes. This 3% release difference further corroborates the presence of a coating. Further release measurements after 24 hours stirring, showed a drastic change in the release percentages for uncoated MOFs. Coated MOFs protected the drug from being released as it increased to 1.5% release. While uncoated MOFs reached up to 10% release in 24 hours.
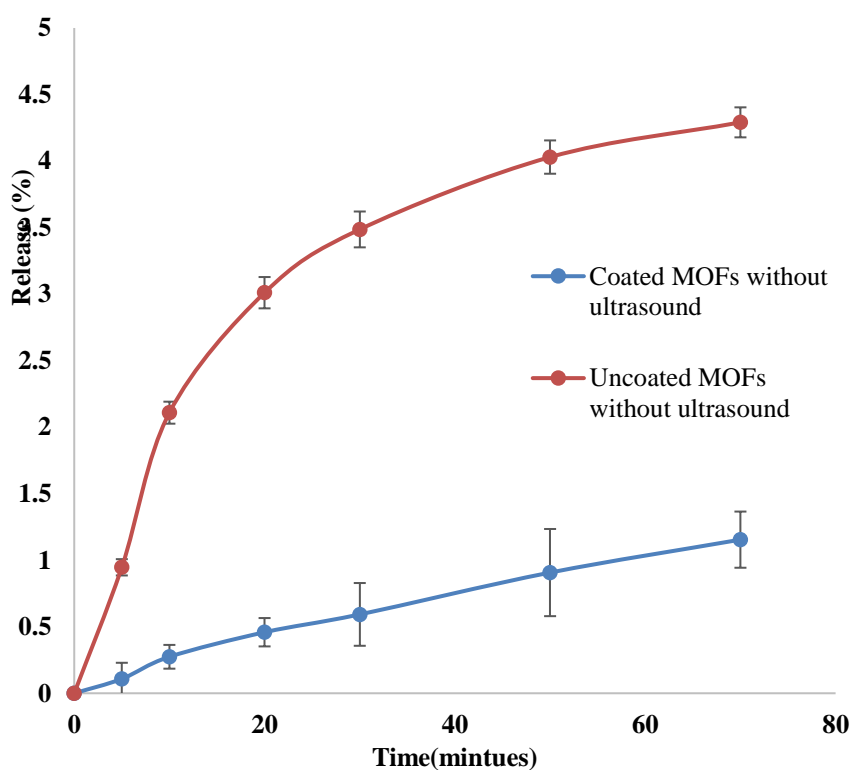
54

Figure 20: Normalized release profiles of uncoated and coated Fe-BTC MOFs without the use of ultrasound. Results reported are the average of three trials ± standard deviation

Note: The fluorescent spectrum for the release is shown in Figures 49 to Figure 54 in the Appendix.

5.8. Release Experiments of Uncoated and Coated Fe-BTC MOFs with Ultrasound

Based on the results presented in the previous section, it is clear that without the use of a trigger mechanism, release from uncoated and coated Fe-BTC MOFs was miniscle. Thus, the use of ultrasound was utilized to enhance the release. Acoustic waves have been extensively used in assisting drug release from liposomes whether based on mechanical or thermal effects. Several other methods have been reported in literature to stimulate drug release including pH, pressure, light and magnetic fields [89]. However, regardless of the stimulus, the release efficiency was significantly low, and required days to reach significant release percentage. It is important to note that the effect of ultrasound on drug release kinetics from MOFs has not been studied or reported in literature. Table 10 summarizes some of these studies.

Table 10: Comparison of different drug release trigger mechanisms from MOFs.

Type of MOFs	Drug	Stimulus	Release efficiency	Reference
ZIF-8	DOX	pH	100% in 10 days at pH 7.4	[90]
MIL-100(Al) gels	DOX	pH	90% in 100 hours at pH 5.5	[91]
Fe-NMOF	DOX	Magnetic	90% in 15 days	[92]
MIL-100(Fe)	DOX	Infrared radiation (IR)	70.4% in 2 hours at pH 5.0	[93]

The US triggered release profiles are shown in Figure 21. Uncoated MOFs showed an increase in release percentages with time reaching to ~50% release at 30 minutes. This can be explained by the cavitation effects generated by ultrasound near the pores of the MOFs, hence the drug is released and some of the pores are disintegrated. The plateau behavior of the release profile of uncoated MOFs, is explained by the fact that they are less sonosensitive compared to coated MOFs, consequently more exposure time or higher frequency of US maybe required to induce more acoustic effect that can break the pore bonds.

The release of the coated Fe-BTC MOFs is lower than the uncoated MOFs up to 30 minutes. As coated MOFs have another lipid bilayer inducing extra resistance for mass diffusion, hence the ultrasound has to induce cavitation in the lipid bilayer, then the MOFs surface. The gradual increase in drug release of uncoated MOFs with each US pulsation, is attributable to the cavitation effect of US. Hence, at each pulsation ,transient pores are formed on the liposomes surface, in which the drug diffuses out through them [70] .

The coated MOFs showed an overall higher release with time compared to uncoated MOFs.This can be explained by several reasons. First, the addition of DSPE-PEG2000-NH$_2$ made the MOFs more sonosensitive according to recently reported studies [94]. Second, the lipid bilayer used to synthesize the liposomes has a neutral charge whereas loaded MOFs are negatively charged. Due to the electrostatic charge interaction, the calcein is further released. The electrostatic force interaction combined with the ultrasound cavitation effect is inducing higher drug release reaching up to 70%.

Furthermore, after 24 hours of stirring, uncoated MOFs showed an increase of 3% in release, as diffusion drives the drug from inside the pores to the releasing medium. Yet, the coated MOFs release increased up to 72%. This is mainly due to release of some ruptured coated MOFs by the stirrer.
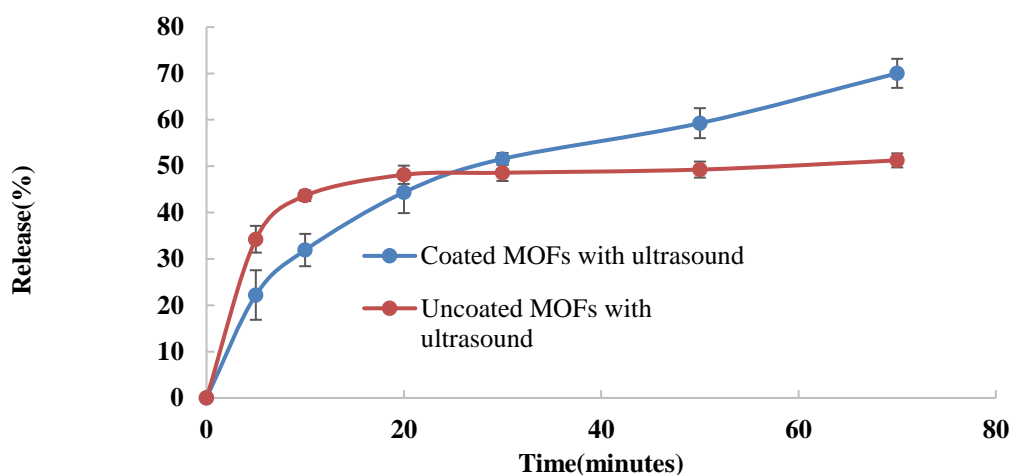

Figure 21: Normalized release profiles of Uncoated and coated Fe-BTC MOFs with the use of ultrasound at 35 kHz. Results reported are the average of three trials ± standard deviation.

Note: The fluorescent spectrum for the release is shown in the Appendix as Figure 55 to Figure 60.

5.9.   Comparison of Release Experiments for Uncoated and Coated Fe-BTC MOFs

The previous sections were comparing the release profiles of uncoated MOFs *vs.* coated MOFs. This section will illustrate the impact of ultrasound on the drug release regardless of the carriers' type. Figure 22 indicates clearly the pronounced effect of ultrasound triggered drug release compared to normal diffusion-driven drug release. The ultrasound triggered release reached up to 70% compared to almost 1.2% in coated MOFs. Even in uncoated MOFs, the maximum release obtained was 4.3%, compared to the ultrasound triggered release that reached a maximum of 54% in the same time period.

In addition, comparing ultrasound as a drug triggering stimulus to other triggering mechanisms shows that acoustic waves have drastically improved the release efficiency, and that whether coated or uncoated within the first 20 minutes, almost 45%

57

of the drug is released. Other stimuli are compared to 20 minutes of ultrasound exposure, are shown in Table 11.
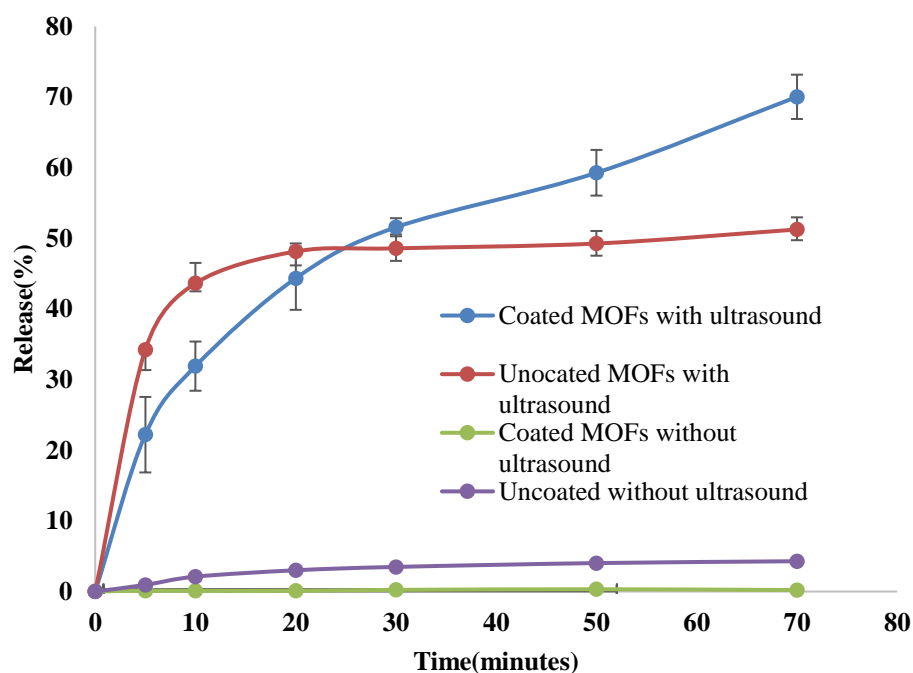

Figure 22: Normalized release profiles of uncoated and coated Fe-BTC MOFs with and without the use of ultrasound. Results reported are the average of three trials ± standard deviation.

Table 11: Comparison of different drug release stimuli from MOFs after 20 minutes of exposure.

Type of MOFs	Drug	Stimulus	Release efficiency	Reference
ZIF-8	DOX	pH	1% in 10 days at pH 7.4	[90]
Fe-NMOF	DOX	Magnetic	1%	[92]
MIL-100(Fe)	DOX	Infrared radiation (IR)	17%	[93]
present work	Calcein	Ultrasound	45%	-

5.10. Impact of Ultrasound on Fe-BTC MOFs

To determine the effect of ultrasound on the morphology and structure of Fe-BTC MOFs, two characterization tests were performed, namely FTIR and XRD, to identify the change in the MOFs in terms of pores, chemical composition and chemical bonds.

5.10.1. FTIR of unloaded MOFs, loaded MOFs and loaded MOFs after US.

Applying ultrasound as a stimulus to release drug from MOFs showed that the MOFs composition was maintained; however, some pores were lost because some chemical bonds were broken during US. Figure 23 compares the FTIR spectrum of three samples, namely, unloaded MOFs, loaded MOFs and MOFs after acoustic exposure.
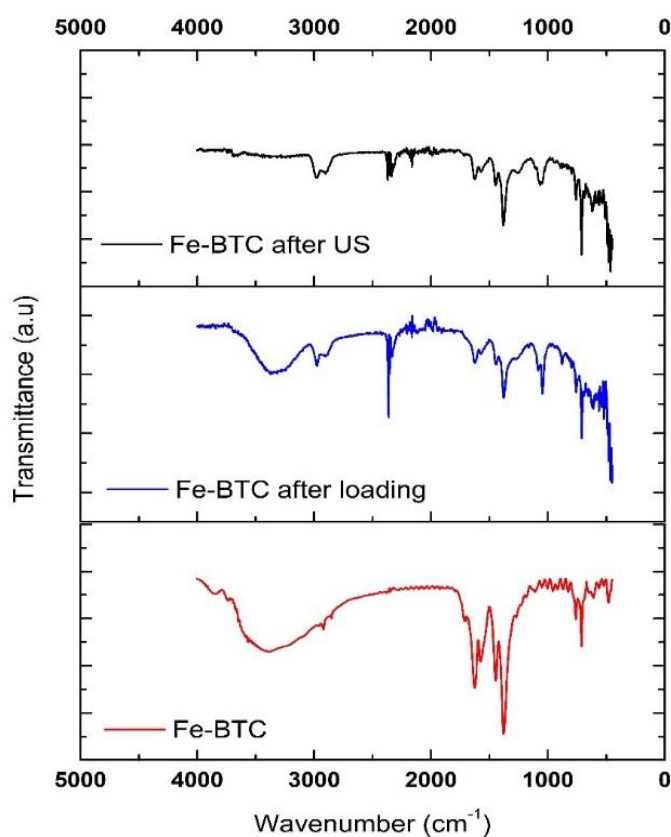
Figure 23: FTIR for Fe-BTC MOFs at several conditions.

The loaded MOFs showed sharper vibrations at 500 cm^{-1} compared to unloaded MOFs, which corresponds to Fe-O bonds that represents the bond between the iron in the MOFs and the oxygen within the calcein. Also, there are notable vibrations at 2300 cm^{-1} in loaded MOFs, which represents isocyanate group (N=C=O), this confirms the

interpore binding of nitrogen from the calcein with the oxygen sites in the MOFs,hence calcein loading into MOFs pores [95].This was followed by several vibrations from 750 cm^{-1} to 1750 cm^{-1} representing the trimesic acid. Some bonds of the loaded MOFs showed similar pattern to unloaded MOFs; specifically, the stretching of O-H bonds at 3200 cm^{-1} and the stretching of C=O at 1750 cm^{-1}. The MOFs after ultrasound exposure showed similar patterns to loaded MOFs, however, several vibrations seem to be altered, which can be explained by the fact that US alters the structure of pores, hence breaking some of the bonds as MOFs are highly flexible. Those vibrations were of O-H bonds at 3200 cm^{-1} and 1500 cm^{-1} which represent the pore bonds that seem to alter in magnitude in the MOFs after US graph.

5.10.2. XRD of loaded MOFs and loaded MOFs after US. XRD patterns of loaded MOFs before and after US agree well with the previously reported images in literature, as shown in Figure 24 [80]. The difference between the loaded MOFs XRD pattern and after US is the higher peak intensity. As the drug is released from the pore, the diffraction pattern yields higher intensity, hence an empty pore [96],[97].Both XRD patterns showed no change in the peaks position ,which confirms that the crystalline structure of the MOFs is maintained .
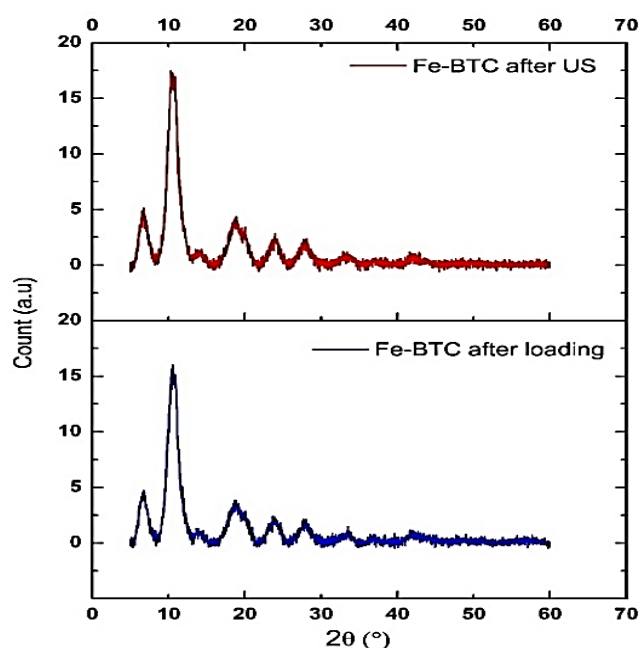

Figure 24: XRD for Fe-BTC MOFs before and after US.

5.11. Statistical Analysis

Several statistical comparisons were performed to study the effect of ultrasound on the drug release from MOFs. A standard two-tailed t-test for unequal variance samples with alpha=0.05 was conducted.

For the t-test:

- The null hypothesis: There is no difference in release percentages with and without ultrasound at the same time point.
- The alternative hypothesis: There is a significant difference in release percentages with and without ultrasound at the same time point.

For each category uncoated and coated MOFs, a t-test was implemented to compare the difference in the drug release percentage at each time point with and without ultrasound as shown in Table 12.

Table 12: The statistical analysis (p-value) of comparing drug release of uncoated and coated MOFs release % without and with US individually.

Type	Uncoated MOFs	Coated MOFs
Time (minutes)	P values comparing release % Without US *vs.* With US	P values comparing release % Without US *vs.* With US
5	1.73×10^{-3}	1.89×10^{-2}
10	2.38×10^{-6}	4.00×10^{-3}
20	2.82×10^{-5}	3.43×10^{-3}
30	7.81×10^{-6}	1.35×10^{-4}
50	7.98×10^{-6}	9.21×10^{-4}
70	3.91×10^{-6}	6.57×10^{-4}
P<0.01	0.01<p<0.05	p>0.05

The calculated p-values shown in Table 10 confirm the presence of a statistically significant difference in the release profiles with and without US as

(p<0.05). Hence, we can reject the null hypothesis and state that the use of ultrasound has significantly improved the model drug release from MOFs.

Another statistical comparison was conducted comparing the US triggered drug release in both categories uncoated and coated MOFs. A standard two-tailed t-test for unequal variance samples with alpha=0.05 was conducted.

For the t-test :

•   The null hypothesis states that there is no difference in release percent for uncoated and coated MOFs under the ultrasound stimulus for drug release at the same time interval.

•   The alternative hypothesis states that there is a significant difference in release percentages for uncoated and coated MOFs under the ultrasound stimulus for drug release at the same time interval.

The calculated (p-values, Table 13) show that at certain time points there is no significant difference in drug released regardless of the drug carrier type, which agrees with the release profiles shown in section 5.8. However, with time the coated liposomes were found to be more sonosensitive. Accordingly, more drug is released and it was evident that there is a significant difference. Overall, the release profiles of US triggered release tend to have similar profiles up to a point in which US becomes inefficient in triggering more drug release from uncoated MOFs, in contrast to coated MOFs that are constantly releasing with US.

Table 13: statistical analysis (p- value) comparing drug release of uncoated and coated MOFs release % with US.

Time (minutes)	P-values comparing release % Without vs. with coating with US vs. With US	
5	4.00×10^{-2}	0.01<p<0.05
10	1.99×10^{-2}	0.01<p<0.05
20	0.279	p>0.05
30	8.41×10^{-2}	p>0.05
50	1.72×10^{-2}	0.01<p<0.05
70	3.05×10^{-3}	P<0.01

5.12. Drug Release Kinetics Mathematical Modelling

The release profiles of uncoated and coated MOFs were fitted into different kinetic models as discussed in section 4.4. The value of the highest coefficient of determination (R^2) was the criterion used to identify whether the data fit the proposed model. Figure 25 to Figure 33 show the modeling profiles for coated MOFs. Figure 34 to Figure 41 below show the modeling profiles of uncoated MOFs.
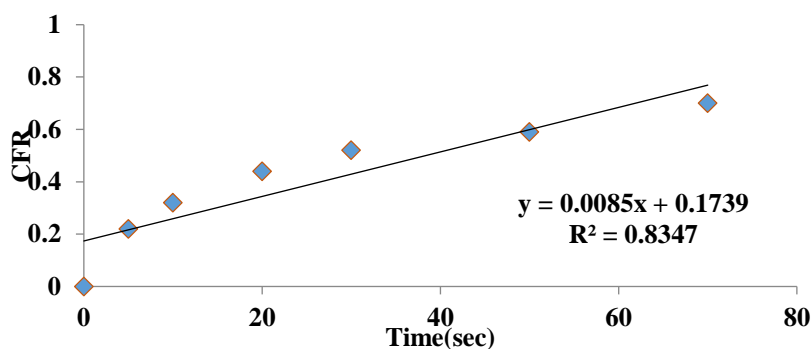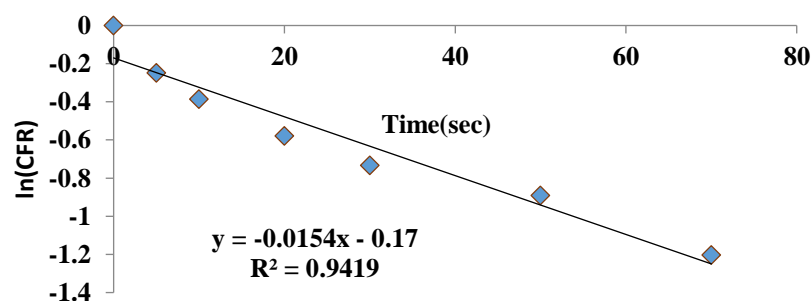

Figure 25: Zero-order model for coated MOFs.

Figure 26: First-order model for coated MOFs.
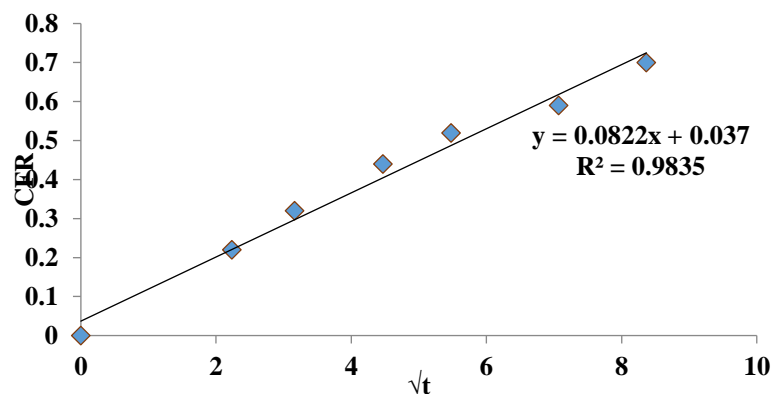
Figure 27: Higuchi model for coated MOFs.

63
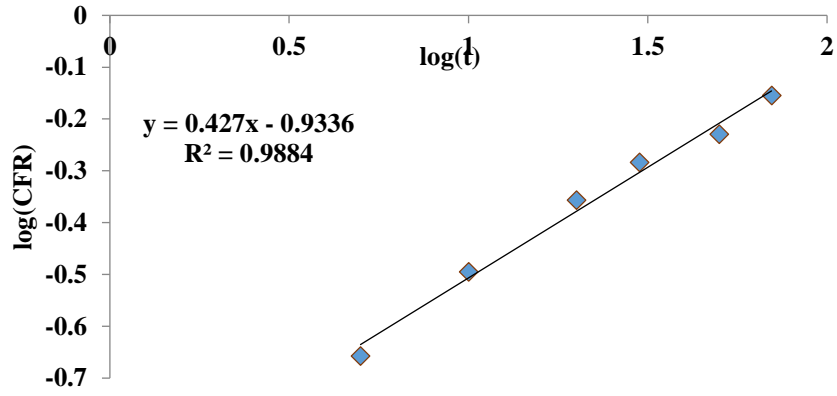
Figure 28: Korsmeyers Peppas model for coated MOFs.
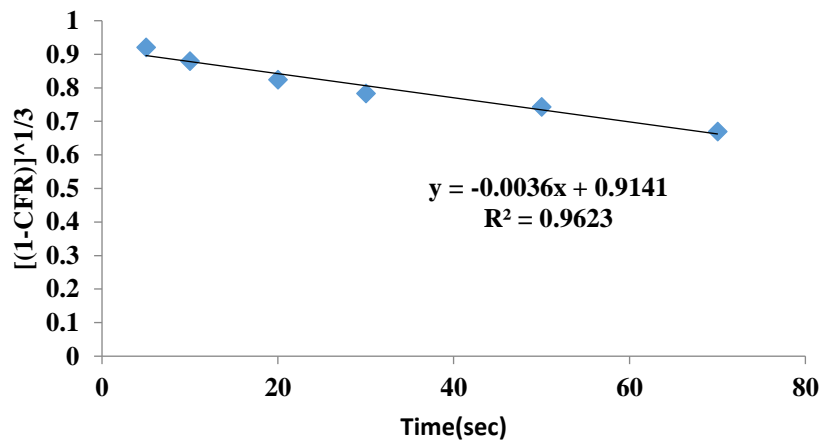
Figure 29: Hixson Crowell model for coated MOFs.
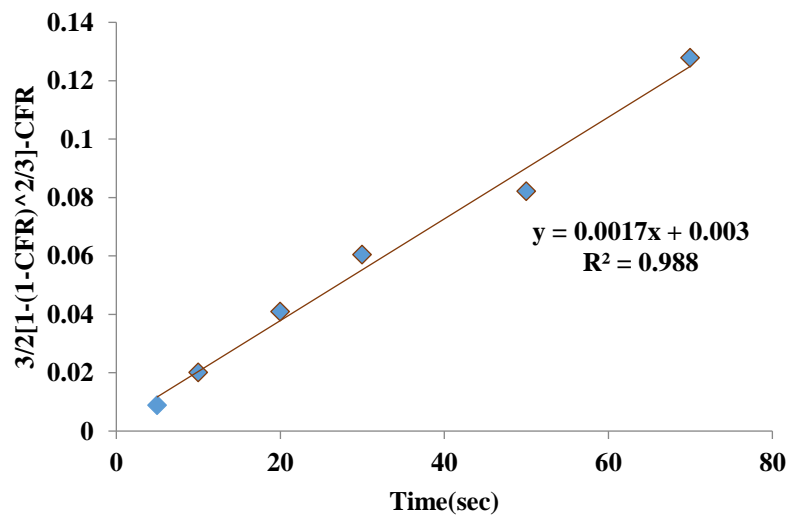
Figure 30: Baker Lonsdale model for coated MOFs.
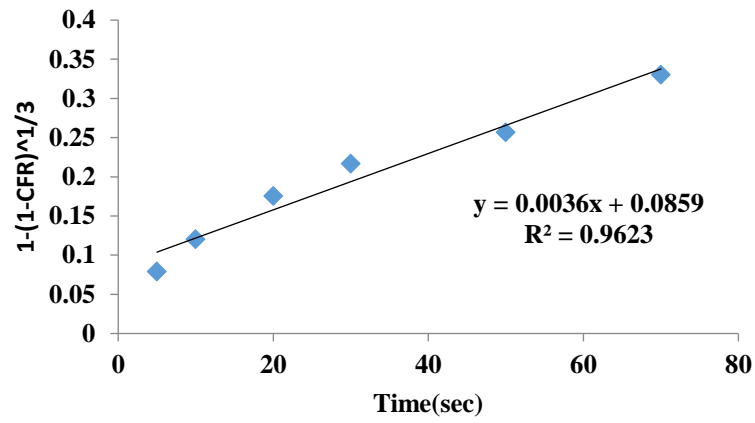
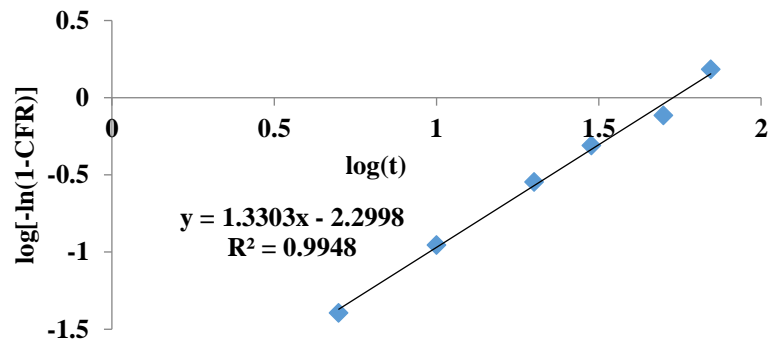Figure 31: Hopfenberg model for coated MOFs.
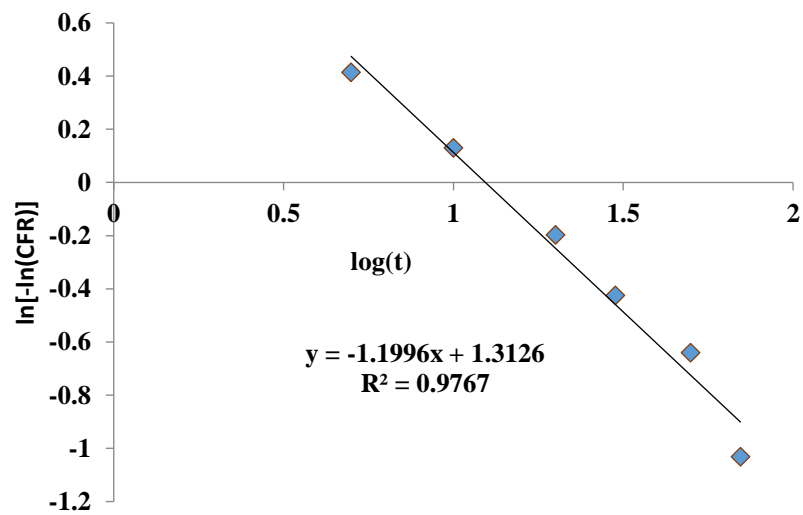

Figure 32: Weibull model for coated MOFs.
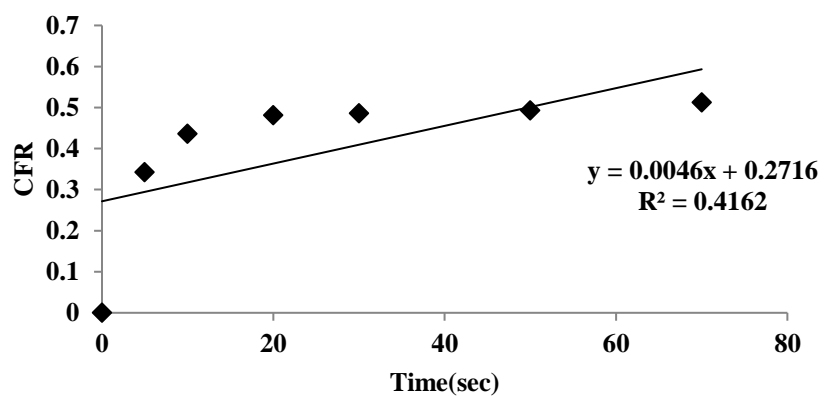

Figure 33: Gompertz model for coated MOFs.
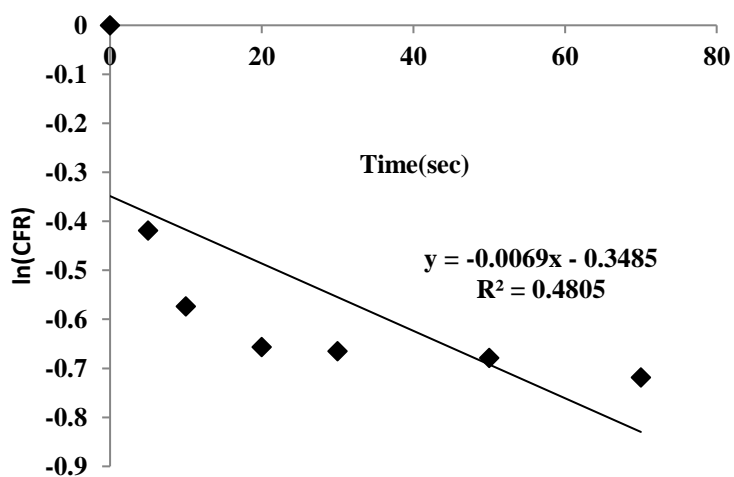
Figure 34: Zero order model for uncoated MOFs.

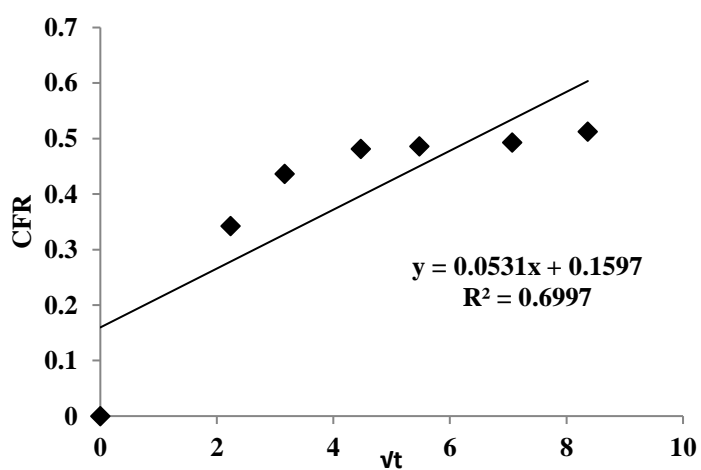Figure 35:First order model for uncoated MOFs.

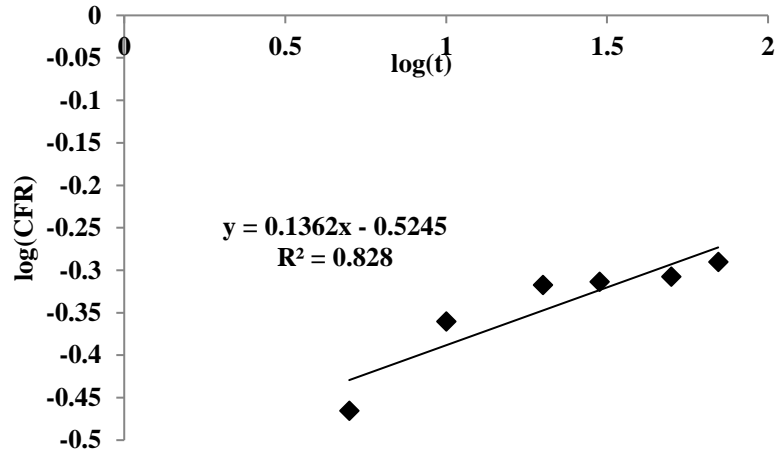Figure 36: Higuchi order model for uncoated MOFs.

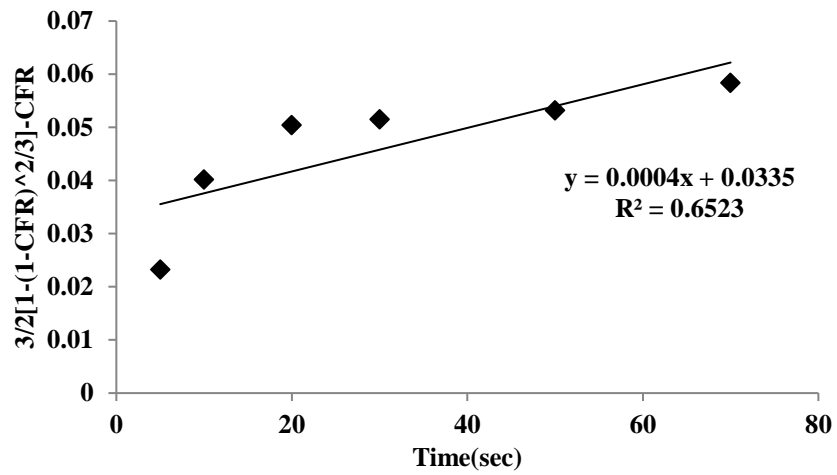Figure 37: Korsmeyer-Peppas model for uncoated MOFs.

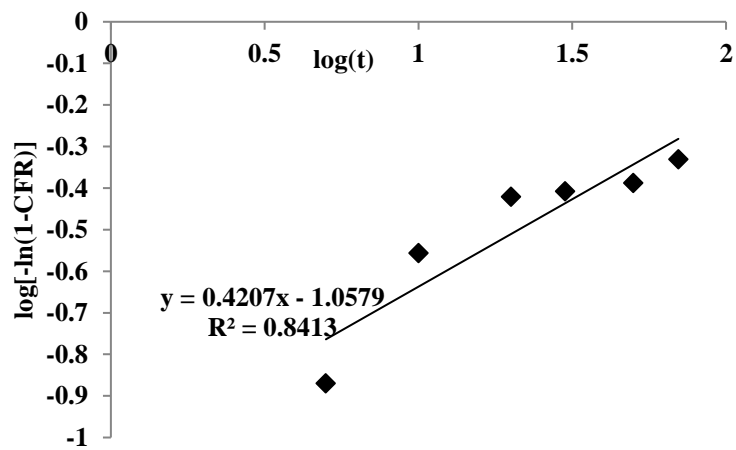Figure 38: Baker-Lonsdale model for uncoated MOFs.

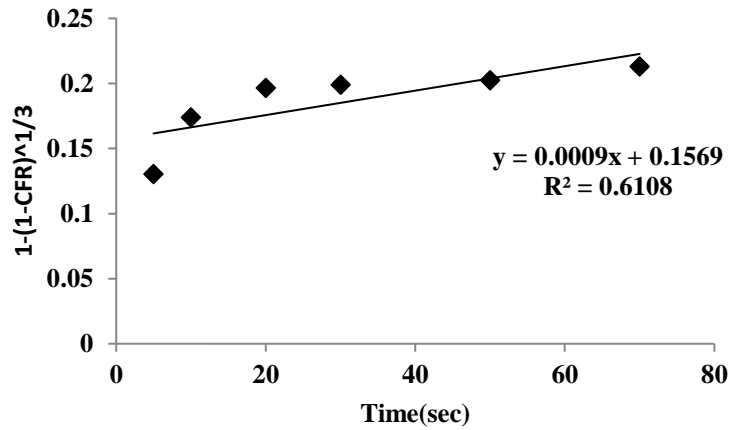Figure 39: Weibull model for uncoated MOFs.

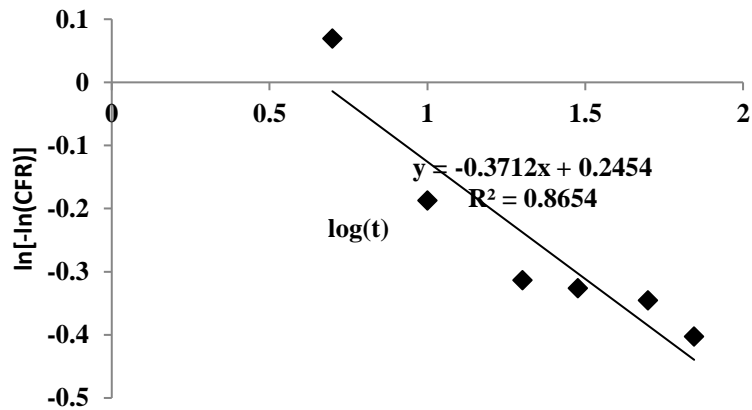Figure 40: Hoffenberg model for uncoated MOFs.

Figure 41:Gompertz model for uncoated MOFs.

The coated MOFs release kinetics were found to agree with most models and with a high value of R^2, namely Korsmeyers Peppas, Baker Lonsdale, Higuchi and Weibull. This concludes that the release mechanism is mainly diffusion-based, as most of these models are controlled by diffusion, hence, according to the diffusion mechanism, drug release takes place in one dimension. There is no swelling or degradation of the nanocarrier and we can use a constant diffusion coefficient for each model [98].

Table 14 compares the coefficient of determination for both uncoated and coated MOFs. Uncoated MOFs seem to fit some models but with relatively low coefficient values. This can be explained because the release profile of uncoated MOFs with US showed almost relatively low changes in the release and almost plateaued after around 30 minutes. The previous models are all based on the concept that there is a

continuous release with time. Since in uncoated MOFs the change in amount of drug released was very small, most models were not the best fit for the data. However, Korsmeyers Peppas and Weibull were the most suitable models for uncoated MOFs, which are both empirical correlations that are not governed by a specific release mechanism.

Table 14: R-Squared of the models for uncoated and coated MOFs.

Type \\ Model	Uncoated MOFs (R^2)	Coated MOFs (R^2)
Zero Order	0.416	0.8347
First order	0.4805	0.9419
Higuchi	0.6700	0.9835
Korsmeyers Peppas	0.8280	0.9884
Baker Lonsdale	0.6523	0.9880
Hixson Crowell	0.6108	0.9623
Weibull	0.8413	0.9948
Hopfenberg	0.6108	0.9623
Gompertz	0.8654	0.9767

Chapter 6. Conclusion and Future Work

Cancer is still one of the deadliest diseases ever known to mankind, and most of the research is targeted towards minimizing the side effects of the existing treatment methods. Drug delivery systems can significantly alter the state of cancer treatment. The usage of small-sized particles that can selectively target cancer cells can drastically minimize the side effects compared to the market available treatments.

In this thesis, a hybrid nanocarrier prepared from the fusion of liposomes and Fe- BTC MOFs have been proven to be a promising candidate. This carrier can resolve the premature release of drugs associated with MOFs, achieve a high drug loading capacity and increase the cellular uptake by endocytosis. This hybrid nanocarrier can also advance the fields of both active and passive targeting. The heavier the nanocarrier, the more accumulated in cancer sites it will be and more favored to pass to cancer cells due to enhanced permeability and retention effect. Besides, liposomes surface can be further modified with targeting moieties to reduce the uptake by healthy cells and especially kill cancer cells.

In this thesis the liposomal coating was verified by two aspects, the change of the carrier size in terms of diameter using DLS and imagining techniques (Cryo-TEM). Also, the charge difference in the surface of the nanocarriers was used, with a change from a negative charge of 39.33±0.42 mv for loaded MOFs to a relatively neutral charge of 6.23±0.47 mv for coated MOFs. Release using low-frequency US at 35 kHz showed that it could drastically improve the drug release compared to normal diffusion-based release. As release of coated and uncoated reached up to 70% and 50%, respectively contrast to release without US that reached up to 1% and 4.5% for coated and uncoated MOFs respectively. This improvement was further validated with statistical analysis using t-test, that showed a significantly difference ($p<0.05$). Also, mathematical modeling of the release profiles for coated MOFs showed that they agree with several models namely Korsmeyers Peppas, Baker Lonsdale, Higuchi and Weibull. Unlike uncoated MOFs, that showed low correlation with the kinetic models, as the release profile of uncoated MOFs plateaued with time.

This thesis provided the initial foundation for the coating MOFs and using US to trigger release, however, future work needs to include:

- Optimization of the calcein drug loading into Fe-BTC MOFs, using several parameters such as the weight of the MOFs, calcein solution concentration and the stirring time.

- *In-vitro* tests to compare the cellular uptake of the coated carrier against uncoated MOFs and the prevention of the premature release of the drug.

- Investigate doxorubicin as a drug since it is hydrophobic and is expected to have a higher loading efficiency by Fe-BTC MOFs.

- Study the effect of pH on the release DOX loaded Fe-BTC MOFs of coated MOFs.

- Investigate the encapsulation of other MOFs that might have a higher loading ability such as MIL-53, ZIF-8 etc.

References

[1]   M. Hejmadi, *Introduction to Cancer Biology*, Denmark: Ventus Publishing, 2010. pp. 2-14.

[2]   G. V Sherbet and M. S. Lakshmi, "1 - Introduction," in *The Genetics of Cancer: Genes Associated with Cancer Invasion, Metastasis and Cell Proliferation* G. V Sherbet and M. S. Lakshmi, Eds. London: Academic Press, 1997, pp. 1–3.

[3]   M. Knowles and P. Selby, *Introduction to the Cellular and Molecular Biology of Cancer*,4th ed , UK,OUP Oxford, 2005, pp. 15–26.

.[4]   L. Wilson, P. Bhatnagar, and N. Townsend, "Comparing trends in mortality from cardiovascular disease and cancer in the United Kingdom, 1983-2013: joinpoint regression analysis", *Popul. Health Metr.*, vol. 15, no. 1, p. 23, Jul. 2017.

[5]   Suchitra Bajpai Chaudhary, "Cancer cases to double by 2030 in Middle East", *gulfnews.com*,2018.[Online].Available:https://gulfnews.com/uae/health/cancer-cases-to-double-by-2030-in-middle-east-1.2215775.[Accessed: 02- May- 2018]

[6]   Department of health, "Cancer Facts & Statistics.",2015.[Online].Available: https://www.haad.ae/simplycheck/tabid/140/Default.aspx. [Accessed: 02- May-2018].

[7]   R. T. Skeel and S. N. Khleif, *Handbook of cancer chemotherapy*, 7th Ed,Lippincott Williams & Wilkins, Philadelphia, USA,2011.

[8]   R. Chen, "Polymers in Drug Delivery: Concepts, Developments and Potential ", *in Drug Delivery Systems: Advanced Technologies Potentially Applicable Personalised Treatment,* J. Coelho, Ed. Dordrecht: Springer, Netherlands, 2013, pp. 1–34.

[9]   A. Mitra, C. H. Lee, and K. Cheng, *Advanced Drug Delivery*,1st ed , US: Wiley, 2013.

[10]   R. Sachan and M. Bajpai, "Transdermal drug delivery system: a review", *IJRDPL*, vol. 3, pp. 66–75,2013.

[11]   P. Abhang, M. Momin, M. Inamdar, and S. Kar, "Transmucosal Drug Delivery-An Overview", *Drug Deliv. Lett.*, vol. 4, no. 1, pp. 26–37, 2014.

[12]   A. Nokhodchi and G. P. Martin, *Advances and Challenges in Pulmonary Drug Delivery : Advances and Challenges*, Chicester, UK: John Wiley & Sons, Incorporated, 2015, pp 63-86.

[13]   R. A. Peterfreund and J. H. Philip, "Critical parameters in drug delivery by intravenous infusion", *Expert Opinion on Drug Delivery*, vol. 10, no. 8, pp. 1095–1108, 2013.

[14]   N. Martinho, C. Damgé, and C. P. Reis, "Recent advances in drug delivery systems", *J. Biomater. Nanobiotechnol.*, vol. 2, no. 05, p. 510, 2011.

[15]   P. D. Reddy and D. Swarnalatha, "Recent advances in novel drug delivery systems", *Int. J. PharmTech Res.*, vol. 2, no. 3, pp. 2025–2027, 2010.

[16] F. U. Din, W. Aman, I. Ullah, O. S. Qureshi, O. Mustapha, S. Shafique, and A. Zeb, "Effective use of nanocarriers as drug delivery systems for the treatment of selected tumors", *Int. J. Nanomedicine*, vol. 12, pp. 7291–7309, Oct. 2017.

[17] R. Singh and J. W. Lillard, "Nanoparticle-based targeted drug delivery", *Exp. Mol. Pathol.*, vol. 86, no. 3, pp. 215–223, Jun. 2009.

[18] S. M. Moghimi, A. C. Hunter, and T. L. Andresen, "Factors controlling nanoparticle pharmacokinetics: an integrated analysis and perspectiv"e, *Annu. Rev. Pharmacol. Toxicol.*, vol. 52, pp. 481–503, 2012.

[19] S. Çalış and K. Öztürk-Atar, "Tumor Targeting Strategies", *J Drug Res Dev*, vol. 3, no. 1, pp. 1009–2470, 2017.

[20] S. Nie, "Understanding and overcoming major barriers in cancer nanomedicine", *Nanomedicine (Lond).*, vol. 5, no. 4, pp. 523–528, Jun. 2010.

[21] Y. H. Bae and K. Park, "Targeted drug delivery to tumors: Myths, reality and possibility", *J. Control. Release*, vol. 153, no. 3, pp. 198–205, Aug. 2011.

[22] B. Bahrami, M. Hojjat-Farsangi, H. Mohammadi, E. Anvari, G. Ghalamfarsa, M. Yousefi, and F. Jadidi-Niaragh, "Nanoparticles and targeted drug delivery in cancer therapy", *Immunol. Lett.*, vol. 190, pp. 64–83, 2017.

[23] M. Malekigorji, A. D. M. Curtis, and C. Hoskins, "The use of iron oxide nanoparticles for pancreatic cancer therapy", *J. Nanomedicine Res.*, vol. 1, no. 1, 2014.

[24] M. Srinivasan, M. Rajabi, and S. A. Mousa, "Multifunctional nanomaterials and their applications in drug delivery and cancer therapy", *Nanomaterials*, vol. 5, no. 4, pp. 1690–1703, 2015.

[25] X. Qian, J. Li, R. Wei, H. Lin, and L. Xiong, "Internal and External Triggering Mechanism of 'Smart' Nanoparticle-based DDSs in Targeted Tumor Therapy", *Curr. Pharm. Des.*, vol. 24, no. 15, pp. 1639–1651, 2018.

[26] R. de la Rica, D. Aili, and M. M. Stevens, "Enzyme-responsive nanoparticles for drug release and diagnostics", *Adv. Drug Deliv. Rev.*, vol. 64, no. 11, pp. 967–978, 2012.

[27] M. D. Norris, K. Seidel, and A. Kirschning, "Externally Induced Drug Release Systems with Magnetic Nanoparticle Carriers: An Emerging Field in Nanomedicine", *Adv. Ther.*, vol. 2, no. 1, p. 1800092, 2019.

[28] R. Banerjee, "Liposomes: Applications in Medicine", *J. Biomater. Appl.*, vol. 16, no. 1, pp. 3–21, Jul. 2001.

[29] P. Carnell, S. A. Scientist, and M. Kaszuba, "Characterizing Liposomes for Drug Delivery", vol. 7, no. 4, pp. 1–7, 2017.

[30] A. Akbarzadeh, R. Rezaei-Sadabady, S. Davaran, S. W. Joo, N. Zarghami, Y. Hanifehpour, M. Samiei, M. Kouhi, and K. Nejati-Koshki, "Liposome: classification, preparation, and applications", *Nanoscale Res. Lett.*, vol. 8, no. 1, p. 102, Feb. 2013.

[31] J. Y. Hwang, Z. Li, and X. J. Loh, "Small molecule therapeutic-loaded liposomes as therapeutic carriers: from development to clinical applications", *RSC Adv.*, vol. 6, no. 74, pp. 70592–70615, 2016.

[32] A. Sharma and U. S. Sharma, "Liposomes in drug delivery: Progress and limitations," *Int. J. Pharm.*, vol. 154, no. 2, pp. 123–140, 1997.

[33] M. Yazdani, S. A. Jalali, A. Badiee, S. Shariat, M. Mansourian, L. Arabi, A. Abbasi, Z. Saberi, and M. R. Jaafari, "Stimulation of tumor-specific immunity by p5 HER-2/neu generated peptide encapsulated in nano-liposomes with high phase transition temperature phospholipids", *Curr. Drug Deliv.*, vol. 14, no. 4, pp. 492–502, 2017.

[34] L. P. Tseng, H. J. Liang, T. W. Chung, Y. Y. Huang, and D. Z. Liu, "Liposomes incorporated with cholesterol for drug release triggered by magnetic field", *J. Med. Biol. Eng.*, vol. 27, no. 1, pp. 29–34, 2007.

[35] M. M. Sandeep Kalepu, Sunilkumar K T, Sudheer Betha, "Lipossomal drug delivery system - A comprehensive review", *Int. J. Drug Dev. Res.*, vol. 5, no. 4, pp. 62–75, 2013.

[36] D. Baczynska, K. Widerak, M. Ugorski, and M. Langner, "Surface charge and the association of liposomes with colon carcinoma cells", *Zeitschrift für Naturforsch. C*, vol. 56, no. 9–10, pp. 872–877, 2001.

[37] L. Sercombe, T. Veerati, F. Moheimani, S. Y. Wu, A. K. Sood, and S. Hua, "Advances and Challenges of Liposome Assisted Drug Delivery", *Front. Pharmacol.*, vol. 6, p. 286, Dec. 2015.

[38] C. Kelly, C. Jefferies, and S.-A. Cryan, "Targeted liposomal drug delivery to monocytes and macrophages", *J. Drug Deliv.*, vol. 2011, 2011.

[39] X. Wei, B. Shao, Z. He, T. Ye, M. Luo, Y. Sang, X. Liang, W. Wang, S. Luo, S. Yang, S. Zhang, C. Gong, M. Gou, H. Deng, Y. Zhao, H. Yang, S. Deng, C. Zhao, L. Yang, Z. Qian, J. Li, X. Sun, J. Han, C. Jiang, M. Wu, and Z. Zhang "Cationic nanocarriers induce cell necrosis through impairment of Na+/K+-ATPase and cause subsequent inflammatory response", *Cell Res.*, vol. 25, p. 237, Jan. 2015.

[40] O. K. Nag and V. Awasthi, "Surface engineering of liposomes for stealth behavior", *Pharmaceutics*, vol. 5, no. 4, pp. 542–569, Oct. 2013.

[41] M. L. Immordino, F. Dosio, and L. Cattel, "Stealth liposomes: review of the basic science, rationale, and clinical applications, existing and potential", *Int. J. Nanomedicine*, vol. 1, no. 3, pp. 297–315, Sep. 2006.

[42] H. Zhang, "Thin-film hydration followed by extrusion method for liposome preparation", in *Liposomes*, 2nd ed., vol 1522, D'Souza G.,Ed, New York:Humana Press, , 2017, pp. 17–22.

[43] M. Wacker and R. Schubert, "From mixed micelles to liposomes: Critical steps during detergent removal by membrane dialysis", *Int. J. Pharm.*, vol. 162, no. 1, pp. 171–175, 1998.

[44] S. Jain, V. Jain, and S. C. Mahajan, "Lipid Based Vesicular Drug Delivery

Systems", *Adv. Pharm.*, vol. 2014, no. i, pp. 1–12, 2014.

[45] M.-R. Toh and G. N. C. Chiu, "Liposomes as sterile preparations and limitations of sterilisation techniques in liposomal manufacturing", *Asian J. Pharm. Sci.*, vol. 8, no. 2, pp. 88–95, 2013.

[46] S. Khadke, P. Stone, A. Rozhin, J. Kroonen, and Y. Perrie, "Point of use production of liposomal solubilised products", *Int. J. Pharm.*, vol. 537, no. 1, pp. 1–8, 2018.

[47] Y. (Chezy) Barenholz, "Doxil® — The first FDA-approved nano-drug: Lessons learned", *J. Control. Release*, vol. 160, no. 2, pp. 117–134, 2012.

[48] H. Furukawa, K. E. Cordova, M. O'Keeffe, and O. M. Yaghi, "The Chemistry and Applications of Metal-Organic Frameworks", *Science (80-.).*, vol. 341, no. 6149, Aug. 2013.

[49] Y. Li, X. Li, Q. Guan, C. Zhang, T. Xu, Y. Dong, X. Bai, and W. Zhang, Y. Li., "Strategy for chemotherapeutic delivery using a nanosized porous metal-organic framework with a central composite design", *Int. J. Nanomedicine*, vol. 12, pp. 1465–1474, 2017.

[50] T. Simon-Yarza, A. Mielcarek, P. Couvreur, and C. Serre, "Nanoparticles of Metal-Organic Frameworks: On the Road to In Vivo Efficacy in Biomedicine", *Adv. Mater.*, vol. 30, no. 37, pp. 1–15, 2018.

[51] N. Stock and S. Biswas, "Synthesis of metal-organic frameworks (MOFs): Routes to various MOF topologies, morphologies, and composites", *Chem. Rev.*, vol. 112, no. 2, pp. 933–969, 2012.

[52] A. Akbarzadeh, R. Rezaei-Sadabady, S. Davaran, S. W. Joo, N. Zarghami, Y. Hanifehpour, M. Samiei, M. Kouhi, and K. Nejati-Koshki., "Liquid metal–organic frameworks", *Nat. Mater.*, vol. 16, no. 11, pp. 1149–1155, 2017.

[53] T. D. Bennett and A. K. Cheetham, "Amorphous Metal–Organic Frameworks", *Acc. Chem. Res.*, vol. 47, no. 5, pp. 1555–1562, May 2014.

[54] W. Xuan, C. Zhu, Y. Liu, and Y. Cui, "Mesoporous metal–organic framework materials", *Chem. Soc. Rev.*, vol. 41, no. 5, pp. 1677–1695, 2012.

[55] C. Dey, T. Kundu, B. P. Biswal, A. Mallick, and R. Banerjee, "Crystalline metal-Organic frameworks (MOFs): Synthesis, structure and function", *Acta Crystallogr. Sect. B Struct. Sci. Cryst. Eng. Mater.*, vol. 70, no. 1, pp. 3–10, 2014.

[56] G. Demazeau, "Solvothermal processes: Definition, key factors governing the involved chemical reactions and new trends", *Zeitschrift fur Naturforsch. - Sect. B J. Chem. Sci.*, vol. 65, no. 8, pp. 999–1006, 2010.

[57] Y.-R. Lee, J. Kim, and W.-S. Ahn, "Synthesis of metal-organic frameworks: A mini review", *Korean J. Chem. Eng.*, vol. 30, no. 9, pp. 1667–1680, 2013.

[58] N. A. Khan and S. H. Jhung, "Synthesis of metal-organic frameworks (MOFs) with microwave or ultrasound: Rapid reaction, phase-selectivity, and size reduction", *Coord. Chem. Rev.*, vol. 285, pp. 11–23, 2015.

[59] Y. Sun and H.-C. Zhou, "Recent progress in the synthesis of metal-organic frameworks", *Sci. Technol. Adv. Mater.*, vol. 16, no. 5, p. 54202, Sep. 2015.

[60] X. Leng, X. Dong, W. Wang, N. Sai, C. Yang, L. You, H. Huang, X. Yin, and J. Ni,., "Biocompatible Fe-Based Micropore Metal-Organic Frameworks as Sustained-Release Anticancer Drug Carriers", *Molecules*, vol. 23, no. 10, p. 2490, 2018.

[61] J. Liu, L. Zhang, J. Lei, H. Shen, and H. Ju, "Multifunctional Metal–Organic Framework Nanoprobe for Cathepsin B-Activated Cancer Cell Imaging and Chemo-Photodynamic Therapy", *ACS Appl. Mater. Interfaces*, vol. 9, no. 3, pp. 2150–2158, Jan. 2017.

[62] Z. Wu, N. Hao, H. Zhang, Z. Guo, R. Liu, B. He, and S. Li, "Mesoporous iron-carboxylate metal–organic frameworks synthesized by the double-template method as a nanocarrier platform for intratumoral drug delivery", *Biomater. Sci.*, vol. 5, no. 5, pp. 1032–1040, 2017.

[63] B. Illes, S. Wuttke, and H. Engelke, "Liposome-Coated Iron Fumarate Metal-Organic Framework Nanoparticles for Combination Therapy", *Nanomaterials*, vol. 7, no. 11, p. 351, 2017.

[64] S.Wuttke, S. Braig, T. Preiß, A. Zimpel, J. Sicklinger, C. Bellomo, J. O. Rädler, A. M. Vollmar, and T. Bein, "MOF nanoparticles coated by lipid bilayers and their uptake by cancer cells", *Chem. Commun.*, vol. 51, no. 87, pp. 15752–15755, 2015.

[65] J. Yang, X. Chen, Y. Li, Q. Zhuang, P. Liu, and J. Gu, "Zr-Based MOFs Shielded with Phospholipid Bilayers: Improved Biostability and Cell Uptake for Biological Applications", *Chem. Mater.*, vol. 29, no. 10, pp. 4580–4589, May 2017.

[66] J. Liu, X. Jiang, C. Ashley, and C. J. Brinker, "Electrostatically Mediated Liposome Fusion and Lipid Exchange with a Nanoparticle-Supported Bilayer for Control of Surface Charge, Drug Containment, and Delivery.", *J. Am. Chem. Soc.*, vol. 131, no. 22, pp. 7567–7569, Jun. 2009.

[67] J. Lee, Y. Shin, W. Lee, K. Whang, D. Kim, L. P. Lee, J.-W. Choi, and T. Kang., "General and programmable synthesis of hybrid liposome/metal nanoparticles", *Sci. Adv.*, vol. 2, no. 12, Dec. 2016.

[68] E. Oude Blenke, "Strategies for triggered drug release from liposomes: in search of smart lipids and" smart" triggers.", M.S. Thesis, Dep. Pharmaceutics, Utrecht Univ., The Netherlands,2012.

[69] W. G. Pitt, G. A. Husseini, and B. J. Staples, "Ultrasonic drug delivery--a general review," *Expert Opin. Drug Deliv.*, vol. 1, no. 1, pp. 37–56, Nov. 2004.

[70] A. Schroeder, J. Kost, and Y. Barenholz, "Ultrasound, liposomes, and drug delivery: principles for using ultrasound to control the release of drugs from liposomes", *Chem. Phys. Lipids*, vol. 162, no. 1–2, pp. 1–16, 2009.

[71] T. J. Evjen, S. Hupfeld, S. Barnert, S. Fossheim, R. Schubert, and M. Brandl, "Physicochemical characterization of liposomes after ultrasound exposure –

Mechanisms of drug release", *J. Pharm. Biomed. Anal.*, vol. 78–79, pp. 118–122, 2013.

[72] H. Kassassir, K. Siewiera, T. Przygodzki, M. Labieniec-Watala, and C. Watala, "Only the Truth Would Enlighten Us—The Advantages and Disadvantages of Flow Cytometry as a Method of Choice in the Study of Mouse and Rat Platelets", *Flow Cytom. Sel. Top.*, p. 31, 2016.

[73] M. Tenopoulou, T. Kurz, P.-T. Doulias, D. Galaris, and U. T. Brunk, "Does the calcein-AM method assay the total cellular 'labile iron pool' or only a fraction of it? ", *Biochem. J.*, vol. 403, no. 2, pp. 261–266, Apr. 2007.

[74] J. K. Patra, G. Das, L. F. Fraceto, E. V. R. Campos, M. D. P. Rodriguez-Torres, L. S. Acosta-Torres, L. A. Diaz-Torres, R. Grillo, M. K. Swamy, S. Sharma, S. Habtemariam, and H.-S. Shin, "Nano based drug delivery systems: recent developments and future prospects", *J. Nanobiotechnology*, vol. 16, no. 1, p. 71, 2018.

[75] M. Foote, "The importance of planned dose of chemotherapy on time: do we need to change our clinical practice?", *Oncologist*, vol. 3, no. 5, pp. 365–368, 1998.

[76] R. Gouda, H. Baishya, and Z. Qing, "Application of mathematical models in drug release kinetics of carbidopa and levodopa ER tablets", *J. Dev. Drugs*, vol. 6, no. 02, 2017.

[77] S. Dash, P. N. Murthy, L. Nath, and P. Chowdhury, "Kinetic modeling on drug release from controlled drug delivery systems", *Acta Pol Pharm*, vol. 67, no. 3, pp. 217–223, 2010.

[78] V. Papadopoulou, K. Kosmidis, M. Vlachou, and P. Macheras, "On the use of the Weibull function for the discernment of drug release mechanisms", *Int. J. Pharm.*, vol. 309, no. 1, pp. 44–50, 2006.

[79] D. Kapoor, R. Maheshwari, K. Verma, S. Sharma, A. Pethe, and R. K. Tekade, "Chapter 1 - Fundamentals of diffusion and dissolution: dissolution testing of pharmaceuticals", in *Advances in Pharmaceutical Product Development and Research*, , 1st ed,R. K. Tekade, Ed. Academic Press, 2020, pp. 1–45.

[80] M. Du, L. Li, M. Li, and R. Si, "Adsorption mechanism on metal organic frameworks of Cu-BTC, Fe-BTC and ZIF-8 for CO2capture investigated by X-ray absorption fine structure", *RSC Adv.*, vol. 6, no. 67, pp. 62705–62716, 2016.

[81] X. Hu, X. Lou, C. Li, Y. Ning, Y. Liao, Q. Chen, E. S. Mananga, M. Shen, and B. Hu,, "Facile synthesis of the Basolite F300-like nanoscale Fe-BTC framework and its lithium storage properties", *RSC Adv.*, vol. 6, no. 115, pp. 114483–114490, 2016.

[82] A. R. Oveisi, A. Khorramabadi-zad, and S. Daliran, "Iron-based metal–organic framework, Fe(BTC): an effective dual-functional catalyst for oxidative cyclization of bisnaphthols and tandem synthesis of quinazolin-4(3H)-ones", *RSC Adv.*, vol. 6, no. 2, pp. 1136–1142, 2016.

[83] S. A. A. Rizvi and A. M. Saleh, "Applications of nanoparticle systems in drug

delivery technology", *Saudi Pharm. J. SPJ Off. Publ. Saudi Pharm. Soc.*, vol. 26, no. 1, pp. 64–70, Jan. 2018.

[84] O. Garbuzenko, Y. Barenholz, and A. Priev, "Effect of grafted PEG on liposome size and on compressibility and packing of lipid bilayer", *Chem. Phys. Lipids*, vol. 135, no. 2, pp. 117–129, 2005.

[85] J. E. Efome, D. Rana, T. Matsuura, and C. Q. Lan, "Metal–organic frameworks supported on nanofibers to remove heavy metals", *J. Mater. Chem. A*, vol. 6, no. 10, pp. 4550–4555, 2018.

[86] J. W. Furry, "Preparation, properties and applications of Calcein in a highly pure form", Ph.D dissertation, Dept. Chem., Iowa State Univ., Iowa,USA,1985.

[87] S. Honary and F. Zahir, "Effect of zeta potential on the properties of nano-drug delivery systems-a review (Part 1) ", *Trop. J. Pharm. Res.*, vol. 12, no. 2, pp. 255–264, 2013.

[88] S. Nimesh, R. Chandra, and N. Gupta, *Advances in nanomedicine for the delivery of therapeutic nucleic acids.*, Cambridge: Woodhead Publishing, 2017.

[89] W. Cai, J. Wang, C. Chu, W. Chen, C. Wu, and G. Liu, "Metal-Organic Framework-Based Stimuli-Responsive Systems for Drug Delivery", *Adv. Sci. (Weinheim, Baden-Wurttemberg, Ger.*, vol. 6, no. 1, p. 1801526, Nov. 2018.

[90] H. Zheng, Y. Zhang, L. Liu, W. Wan, P. Guo, A. M. Nyström, and X. Zou., "One-pot Synthesis of Metal–Organic Frameworks with Encapsulated Target Molecules and Their Applications for Controlled Drug Delivery", *J. Am. Chem. Soc.*, vol. 138, no. 3, pp. 962–968, Jan. 2016.

[91] Y. Feng, C. Wang, F. Ke, J. Zang, and J. Zhu, "MIL-100(Al) Gels as an Excellent Platform Loaded with Doxorubicin Hydrochloride for pH-Triggered Drug Release and Anticancer Effect.", *Nanomater. (Basel, Switzerland)*, vol. 8, no. 6, Jun. 2018.

[92] K. Sethi, S. Sharma, and I. Roy, "Nanoscale iron carboxylate metal organic frameworks as drug carriers for magnetically aided intracellular delivery", *RSC Adv.*, vol. 6, no. 80, pp. 76861–76866, 2016.

[93] Y.. Zhu, S.-P. Chen, H. Zhao, Y. Yang, X.-Q. Chen, J. Sun, H.-S. Fan, and X.D. Zhang,, "PPy@MIL-100 Nanoparticles as a pH- and Near-IR-Irradiation-Responsive Drug Carrier for Simultaneous Photothermal Therapy and Chemotherapy of Cancer Cells", *ACS Appl. Mater. Interfaces*, vol. 8, no. 50, pp. 34209–34217, Dec. 2016.

[94] N. Awad *et al.*, "The effect of pegylation and targeting moieties on the ultrasound-mediated drug release from liposomes", *ACS Biomater. Sci. Eng.*, Jun. 2019.

[95] K. B. H. Badri, W. C. Sien, M. Shahrom, L. C. Hao, N. Y. Baderuliksan, and N. R. Norzali, "FTIR spectroscopy analysis of the prepolymerization of palm-based polyurethane", *Solid State Sci. Technol*, vol. 18, no. 2, pp. 1–8, 2010.

[96] L. J. Waters, J. P. Hanrahan, J. M. Tobin, C. V. Finch, G. M. Parkes, S. A. Ahmad, F. Mohammad, and M. Saleem, "Enhancing the dissolution of

phenylbutazone using Syloid® based mesoporous silicas for oral equine applications", *J. Pharm. Anal.*, vol. 8, no. 3, pp. 181–186, 2018.

[97]   K. Varaprasad, K. Vimala, S. Ravindra, N. Narayana Reddy, G. Siva Mohana Reddy, and K. Mohana Raju, "Biodegradable Chitosan Hydrogels for In Vitro Drug Release Studies of 5-Flurouracil an Anticancer Drug", *J. Polym. Environ.*, vol. 20, no. 2, pp. 573–582, 2012.

[98]   Y. Fu and W. J. Kao, "Drug release kinetics and transport mechanisms of non-degradable and degradable polymeric delivery systems", *Expert Opin. Drug Deliv.*, vol. 7, no. 4, pp. 429–444, Apr. 2010.

Appendix

		Size (d.nm):	% Intensity:	St Dev (d.nm):
Z-Average (d.nm): 162.5	Peak 1:	180.7	100.0	60.96
PdI: 0.090	Peak 2:	0.000	0.0	0.000
Intercept: 0.962	Peak 3:	0.000	0.0	0.000
Result quality : Good				

Size Distribution by Intensity
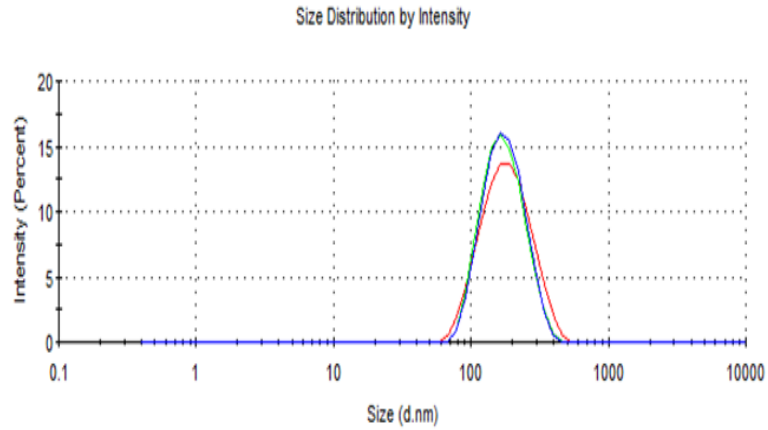
Figure 42: Size distribution for coated MOFs.

		Size (d.nm):	% Intensity:	St Dev (d.nm):
Z-Average (d.nm): 149.8	Peak 1:	165.9	98.6	63.42
PdI: 0.169	Peak 2:	4964	1.4	625.0
Intercept: 0.962	Peak 3:	0.000	0.0	0.000
Result quality : Good				

Size Distribution by Intensity
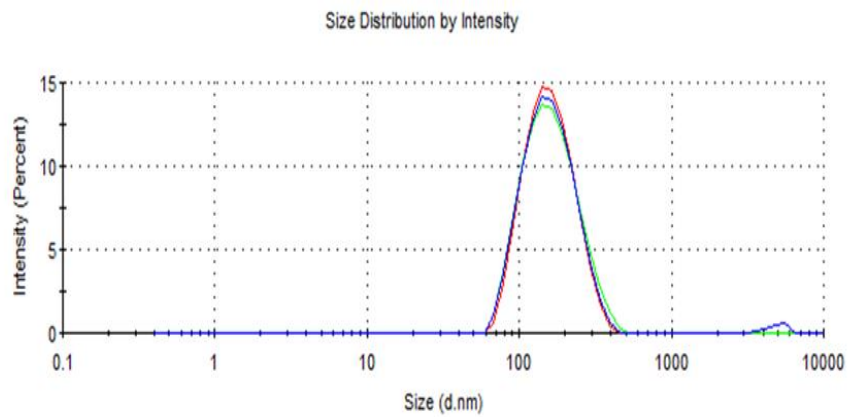
Figure 43: Size distribution for liposomes.

80
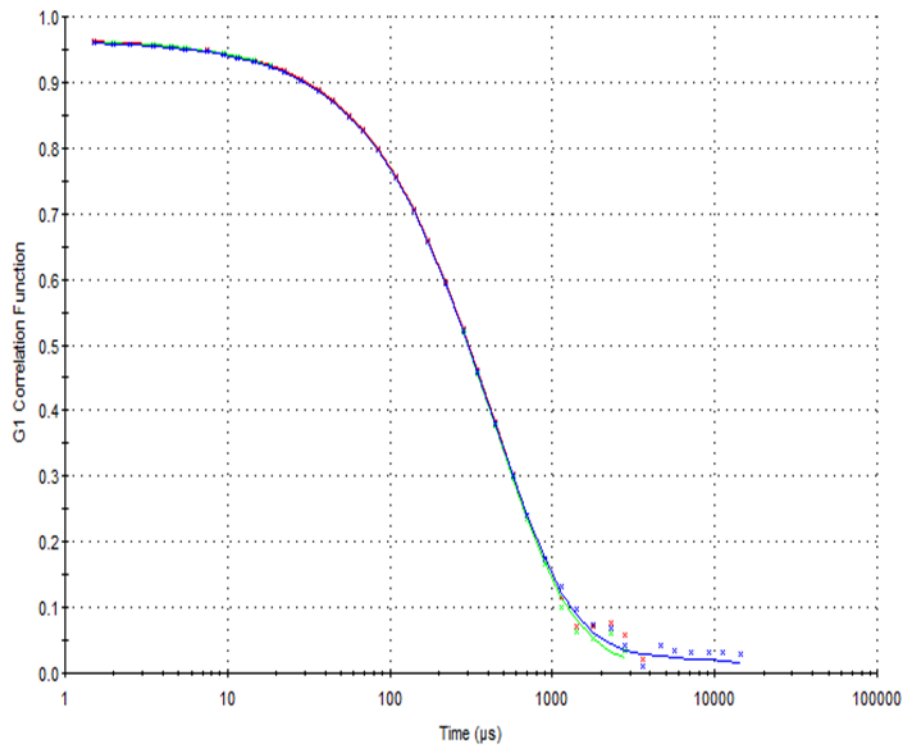
Figure 44: Cross correlation for Coated MOFs.

Data Fit
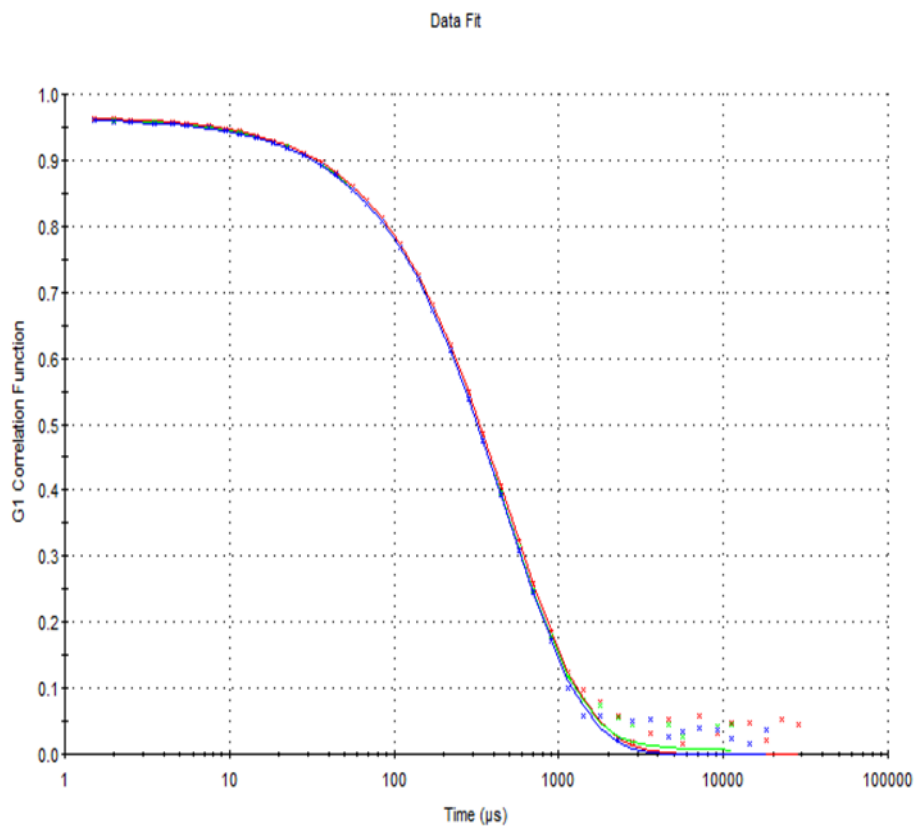
Figure 45: Cross correlation for liposomes.

		Mean (mV)	Area (%)	St Dev (mV)
Zeta Potential (mV): -14.0	Peak 1:	-21.8	72.2	7.93
Zeta Deviation (mV): 17.3	Peak 2:	-1.73	11.6	3.20
Conductivity (mS/cm): 0.0741	Peak 3:	17.0	8.4	4.79
Result quality : See result quality report				
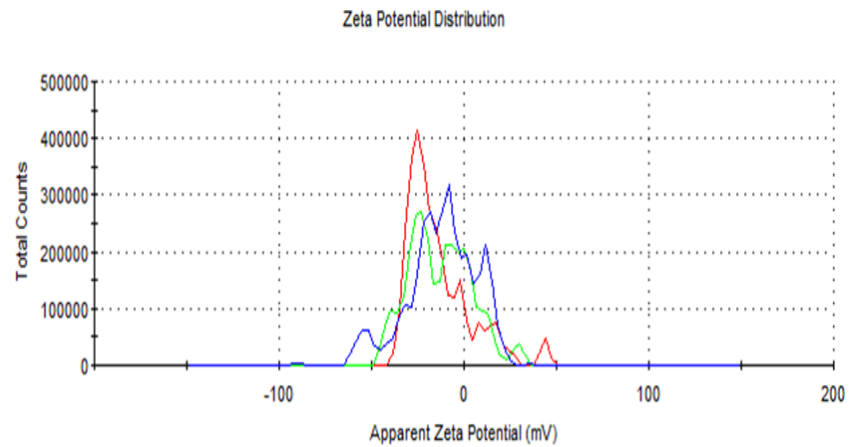
Figure 46: Zeta potential distribution for unloaded MOFs.

		Mean (mV)	Area (%)	St Dev (mV)
Zeta Potential (mV): -39.2	Peak 1:	-39.2	100.0	11.1
Zeta Deviation (mV): 11.1	Peak 2:	0.00	0.0	0.00
Conductivity (mS/cm): 0.0219	Peak 3:	0.00	0.0	0.00
Result quality : See result quality report				
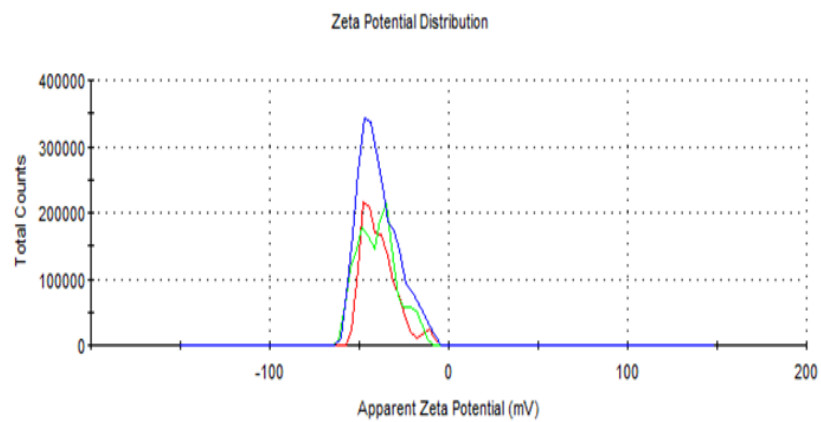
Figure 47: Zeta potential distribution for loaded MOFs.
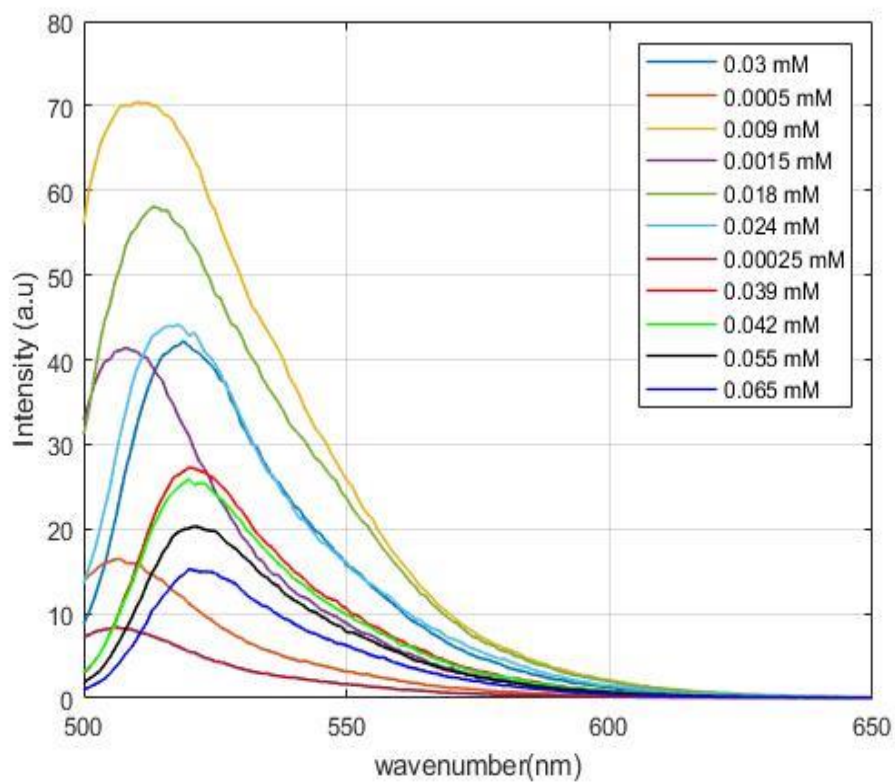
Figure 48: Calibration curve spectrum.
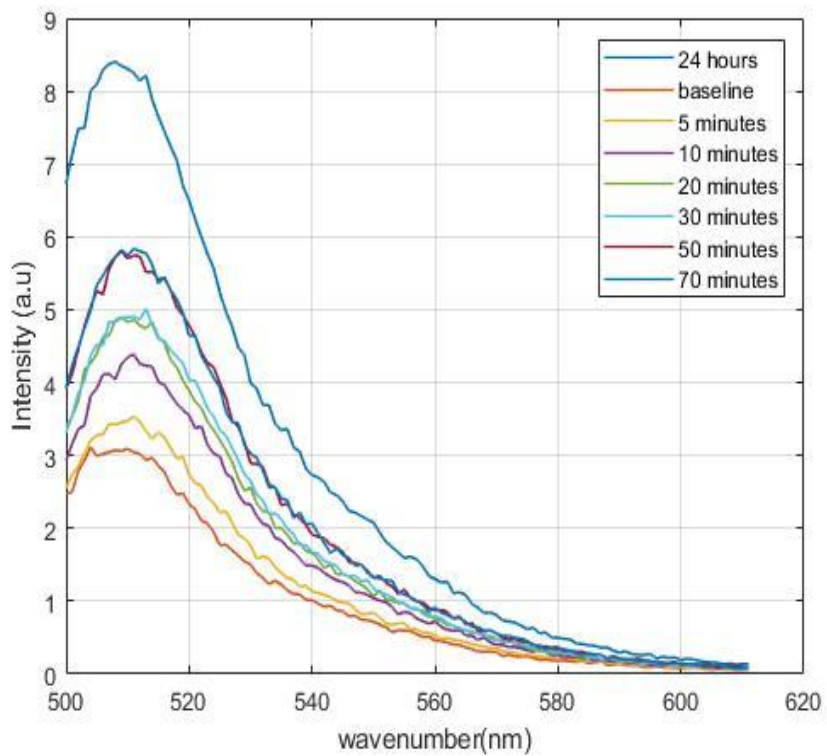
Figure 49: Release without US on uncoated MOFs Trail 1.
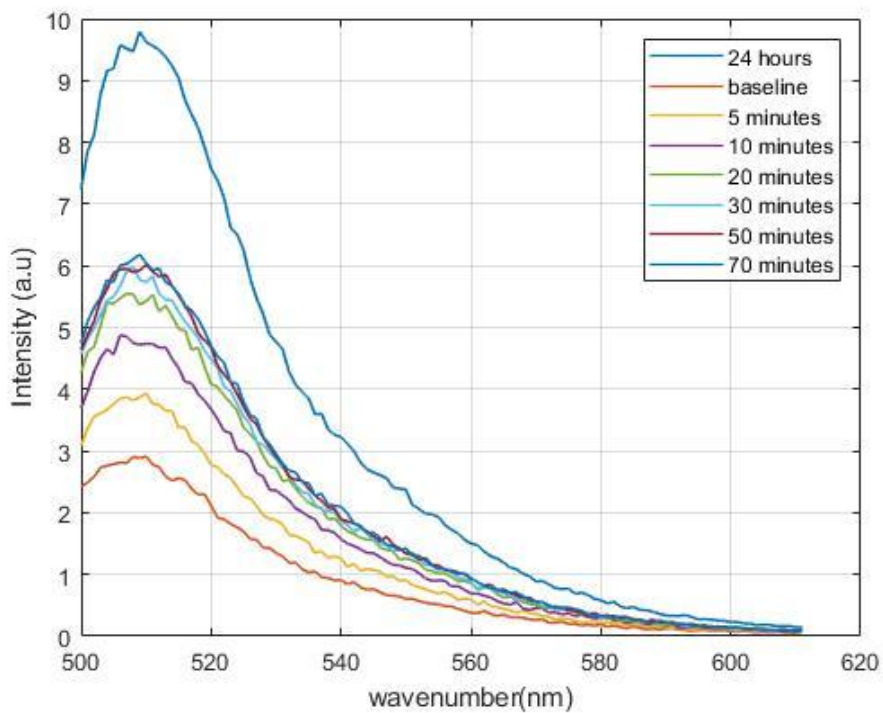
Figure 50 : Release without US on uncoated MOFs Trail 2 .
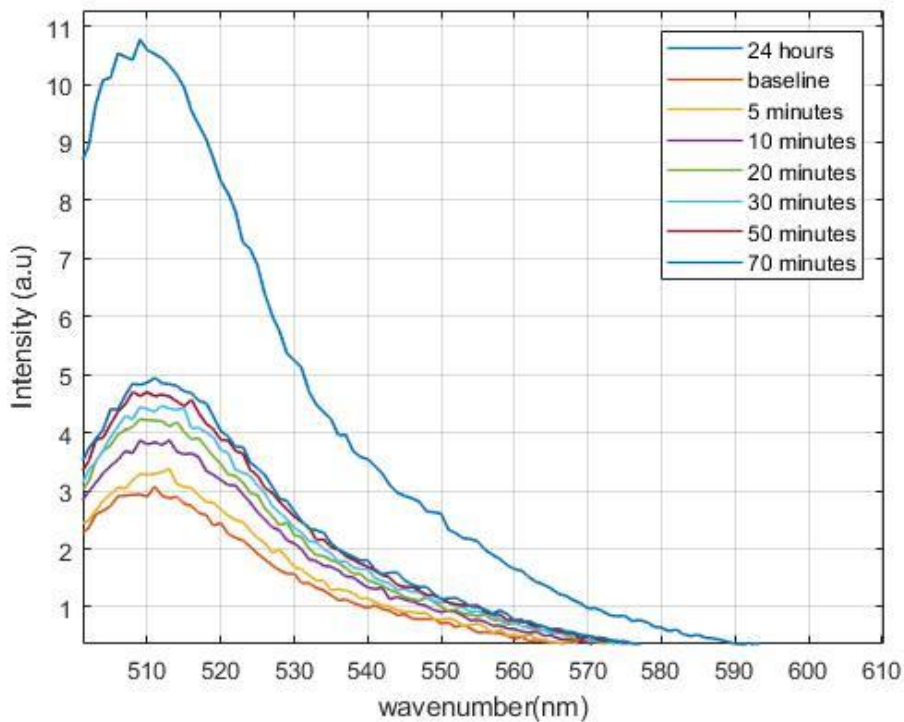
Figure 51: Release without US on uncoated MOFs Trail 3.
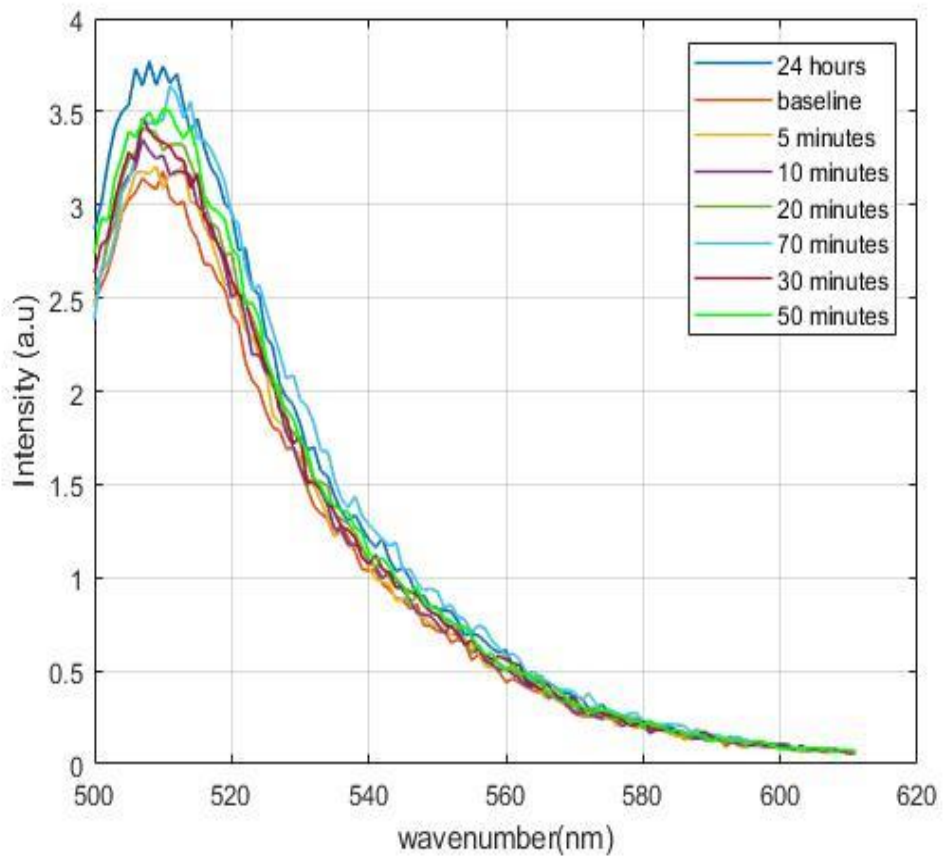
Figure 52:Release without US on coated MOFs Trail 1.
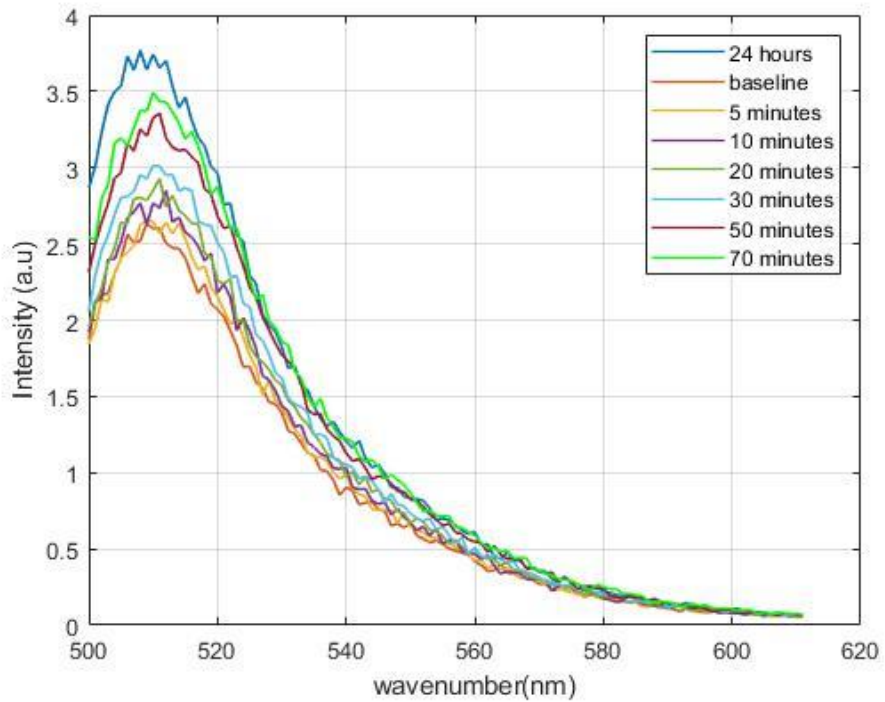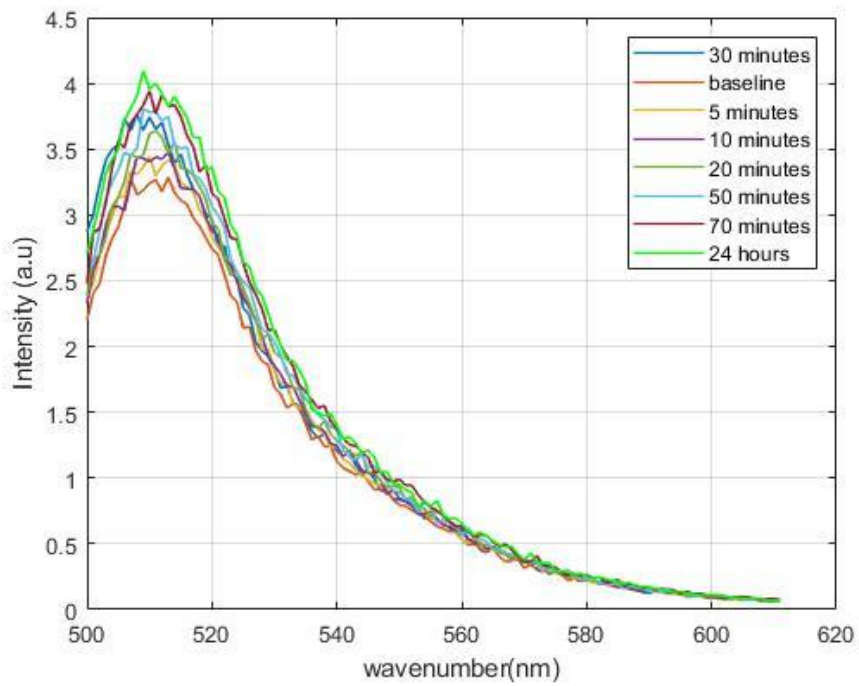

Figure 53: Release without US on coated MOFs Trail 2.

.

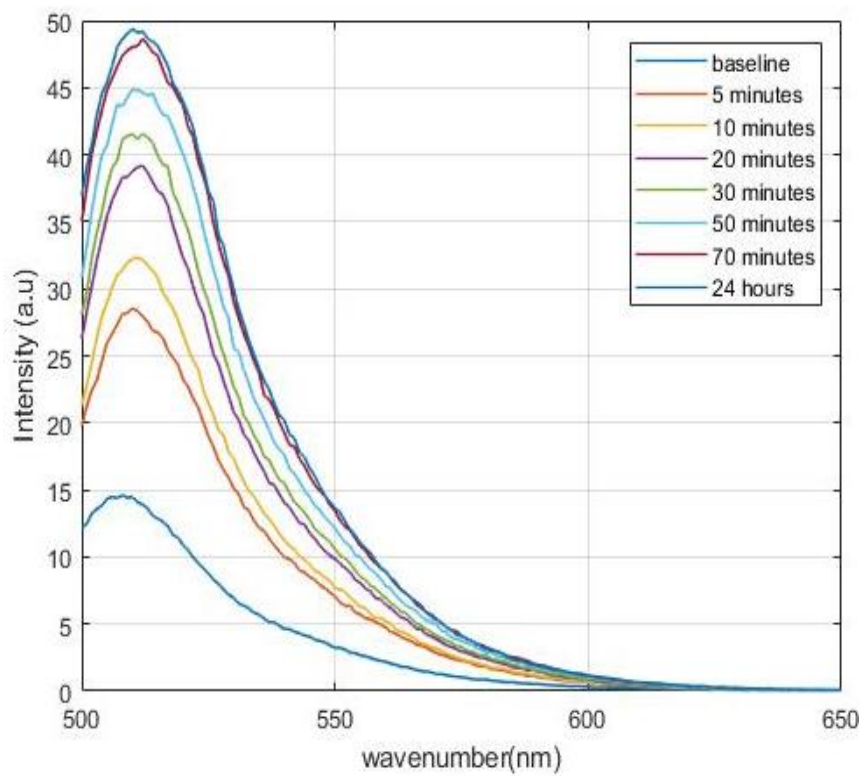
Figure 54: Release without US on coated MOFs Trail 3.

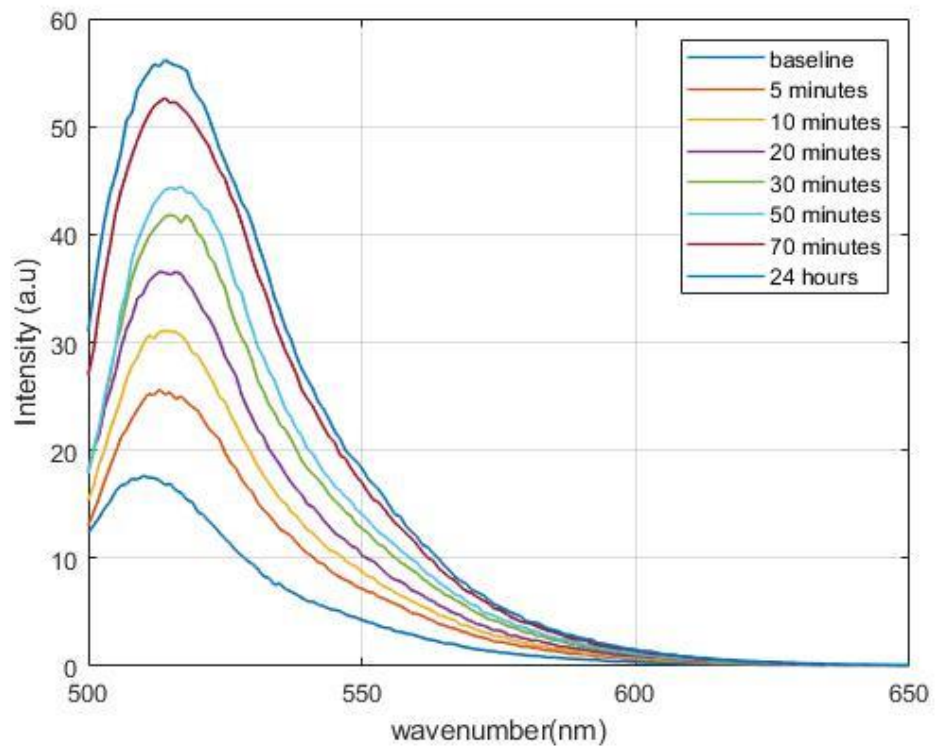Figure 55:Release with US on coated MOFs Trail1
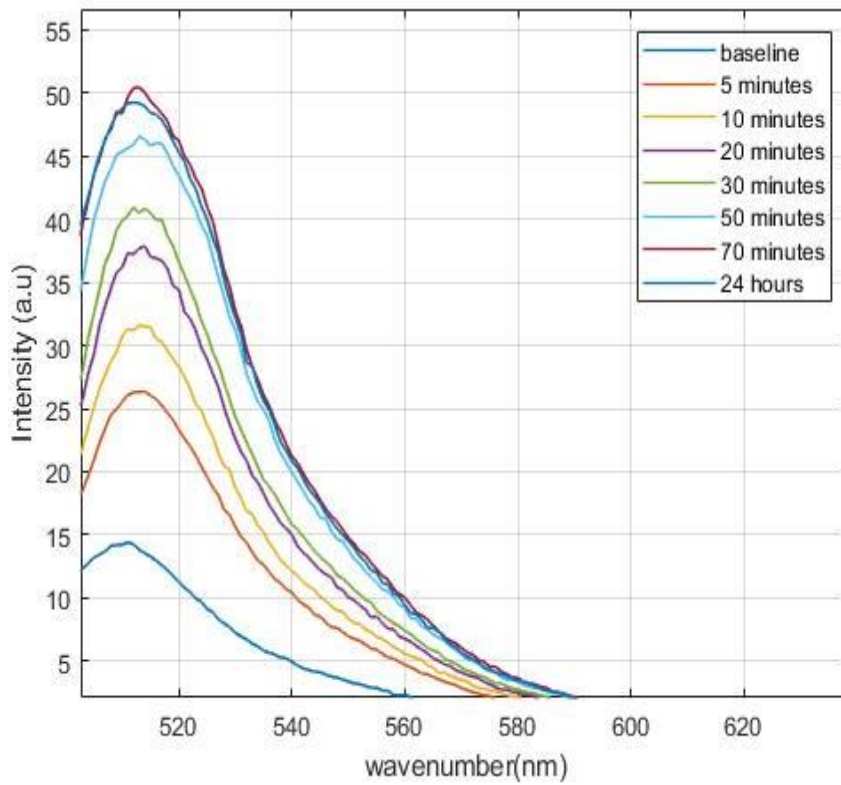
Figure 56:Release with US on coated MOFs Trail 2.

Figure 57:Release with US on coated MOFs Trail 3.
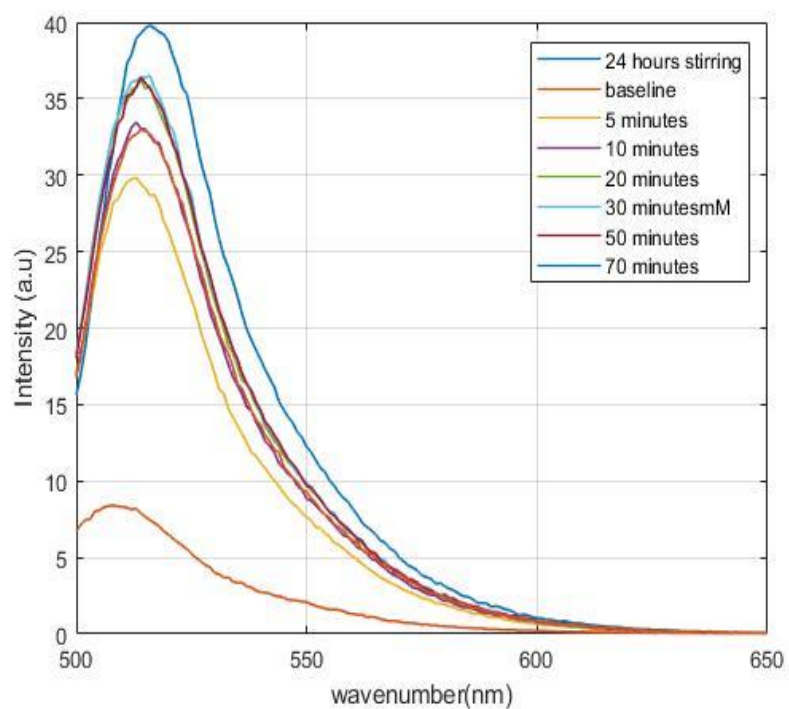
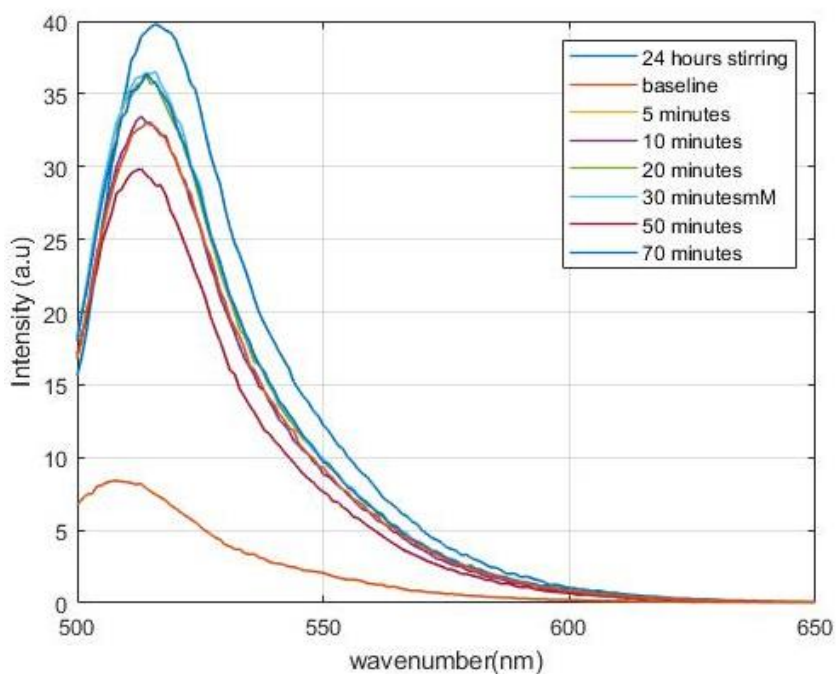Figure 58: Release with US on uncoated MOFs Trail 1.
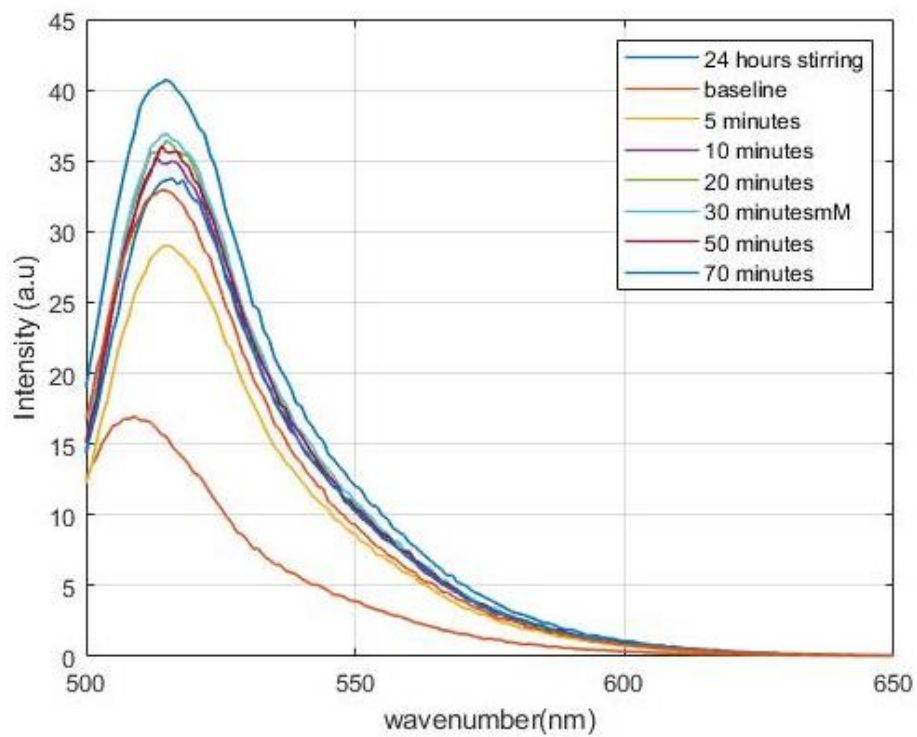

Figure 59: Release with US on uncoated MOFs Trail 2 .

Figure 60: Release with US on uncoated MOFs Trail 3.

Vita

Omnia Mohamed was born in 1994, in Ras Al-Khaimah, United Arab Emirates. She received her elementary and her secondary education from Al shola private school in Sharjah, United Arab Emirates. She received her B.Sc.(honours). degree in Chemical Engineering from University of Khartoum, Sudan in 2016. Also, she was awarded the best academic excellence award for achieving the first rank in her batch. In 2018, she joined the Biomedical Engineering master's program at the American University of Sharjah. She was awarded a graduate assistantship that allowed her to work as a graduate teaching and research assistant from January 2018 till December 2019. She participated and presented her thesis in AUS symposium on biosciences and bioengineering (2017).